

INTERACTION WITH AN OBSTACLE IN THE 2D FOCUSING NONLINEAR SCHRÖDINGER EQUATION

OUSSAMA LANDOULSI, SVETLANA ROUDENKO, AND KAI YANG

ABSTRACT. We present a numerical study of solutions to the $2d$ cubic and quintic focusing nonlinear Schrödinger equation in the exterior of a smooth, compact and strictly convex obstacle (a disk) with Dirichlet boundary condition. We first investigate the effect of the obstacle on the behavior of solutions traveling toward the obstacle at different angles and with different velocities directions. We introduce a new concept of weak and strong interactions of the solutions with the obstacle. Next, we study the existence of blow-up solutions depending on the type of the interaction and show how the presence of the obstacle changes the overall behavior of solutions (e.g., from blow-up to global existence), especially in the strong interaction case, as well as how it affects the shape of solutions compared to their initial data, (e.g., splitting into transmitted and reflected parts). We also investigate the influence of the size of the obstacle on the eventual existence of blow-up solutions in the strong interaction case in terms of the transmitted and the reflected parts of the mass. Moreover, we show that the sharp threshold for global existence vs. finite time blow-up solutions in the mass critical case in the presence of the obstacle is the same as the one given by Weinstein for NLS in the whole Euclidean space \mathbb{R}^d . Finally, we construct new Wall-type initial data that blows up in finite time after a strong interaction with an obstacle and having a very distinct dynamics compared with all other blow-up scenarios and dynamics for the NLS in the whole Euclidean space \mathbb{R}^d .

CONTENTS

1. Introduction	2
2. Numerical approach	7
3. The NLS equation on the whole plane \mathbb{R}^2	13
4. Perturbations of the soliton in the NLS with obstacle	14
5. Dependence on the distance	16
6. Weak interaction with an obstacle	18
7. Strong interaction with an obstacle	26
8. Dependence on the obstacle size	30
9. Blow-up: Wall-type initial data	36
10. Conclusion	40
References	40

2010 *Mathematics Subject Classification.* 35Q55, 58J32, 58J37, 65N06, 35B40, 65M06.

Key words and phrases. Focusing NLS equation, convex obstacle, exterior domain, soliton-obstacle interaction, scattering, blow-up.

1. INTRODUCTION

We consider the $2d$ focusing nonlinear Schrödinger equation (NLS) outside of a smooth, compact and strictly convex obstacle with Dirichlet boundary conditions:

$$\begin{cases} i\partial_t u + \Delta_\Omega u = -|u|^{p-1}u & (t, x) \in \mathbb{R} \times \Omega, \\ u(t_0, x) = u_0(x) & \forall x \in \Omega, \\ u(t, x) = 0 & (t, x) \in \mathbb{R} \times \partial\Omega, \end{cases} \quad (\text{NLS}_\Omega)$$

where $t_0 \in \mathbb{R}$ is the initial time, Ω is an exterior domain in \mathbb{R}^2 and Δ_Ω is the Dirichlet Laplace operator defined by $\Delta_\Omega := \partial_x^2 + \partial_y^2$, $(x, y) \in \mathbb{R}^2$. Here, u is a complex-valued function,

$$\begin{aligned} u : \mathbb{R} \times \Omega &\longrightarrow \mathbb{C} \\ (t, x) &\longmapsto u(t, x). \end{aligned}$$

We consider $u_0 \in H_0^1(\Omega)$, where the Sobolev space $H_0^1(\Omega)$ is the set of functions in $H^1(\Omega)$ that satisfy Dirichlet boundary conditions, i.e., $u = 0$ on $\partial\Omega$.

The NLS_Ω equation is locally well-posed in $H_0^1(\Omega)$ in dimension $d = 2$, see [9], [8] for a non-trapping obstacle and [23], [22] for a strictly convex obstacle. The solution u can be extended to a maximal time interval $I = (-T_-, T_+)$ of existence and the following alternative holds:

either $T_+ = \infty$ (respectively, $T_- = \infty$), or $T_+ < \infty$ (respectively, $T_- < \infty$) with

$$\lim_{t \rightarrow T_+} \|u(t, \cdot)\|_{H_0^1(\Omega)} = \infty \quad \left(\text{respectively, } \lim_{t \rightarrow T_-} \|u(t, \cdot)\|_{H_0^1(\Omega)} = \infty \right).$$

During their lifespans, solutions to the nonlinear Schrödinger equation outside an obstacle conserve both mass and energy:

$$M_\Omega[u(t)] := \int_\Omega |u(t, x)|^2 dx = M_\Omega[u_0], \quad (1.1)$$

$$E_\Omega[u(t)] := \int_\Omega |\nabla u(t, x)|^2 dx - \frac{1}{p+1} \int_\Omega |u(t, x)|^{p+1} dx = E_\Omega[u_0]. \quad (1.2)$$

Unlike the nonlinear Schrödinger equation $\text{NLS}_{\mathbb{R}^d}$ posed on the whole Euclidean space \mathbb{R}^d , the NLS_Ω equation does not preserve the momentum $P_\Omega[u] = \text{Im} \int_\Omega \bar{u}(t, x) \nabla u(t, x) dx$, since the derivative of the momentum P_Ω with respect to the time variable is equal to a non-zero boundary term.

Furthermore, the $\text{NLS}_{\mathbb{R}^2}$ equation, posed on the whole Euclidean space \mathbb{R}^2 , is invariant under the scaling transformation, that is, if $u(t, x)$ is a solution to the $\text{NLS}_{\mathbb{R}^2}$ equation, then $\lambda^{\frac{2}{p-1}} u(\lambda x, \lambda^2 t)$ is also a solution for $\lambda > 0$. This scaling identifies the critical Sobolev space $\dot{H}_x^{s_c}$, where the critical regularity s_c is given by

$$s_c := \frac{p-3}{p-1}.$$

The equation, when $s_c = 0$, is referred to as the mass-critical (or the L^2 -critical), and when $0 < s_c < 1$, is called the mass-supercritical (or L^2 -supercritical) and energy-subcritical (or H^1 -subcritical). Throughout this paper, we consider the $2d$ cubic ($p = 3$) and quintic ($p = 5$) NLS_Ω equations. Since the presence of the obstacle does not change the intrinsic dimensionality of the problem, we may regard the cubic NLS_Ω equation as being the mass-critical equation and the quintic one as the mass-supercritical and energy-subcritical (or intercritical) equation.

The focusing NLS equation, posed on the whole space, admits soliton solutions that are periodic in time, that is, $u(t, x) = e^{it\omega} Q_\omega(x)$, where $\omega > 0$ and Q_ω is an H^1 smooth solution of the nonlinear elliptic equation,

$$-\Delta Q_\omega + \omega Q_\omega = |Q_\omega|^{p-1} Q_\omega. \quad (1.3)$$

In this paper, we denote by Q_ω the ground state solution, that is, the unique, positive, vanishing at infinity H^1 solution of (1.3). The ground state solution turns out to be radial, smooth and exponentially decaying function (for $s_c < 1$), see [10], [18], [4], [29]. Moreover, Q_ω characterized as the unique minimizer for the Gagliardo-Nirenberg inequality up to scaling, space translation and phase shift, see [29]. For simplicity, we denote by Q the ground state solution of (1.3), when $\omega = 1$.

The NLS equation, posed on the whole Euclidean space \mathbb{R}^d , also enjoys Galilean invariance: if $u(t, x)$ is a solution, then so is $u(t, x - vt) e^{i(\frac{x \cdot v}{2} - \frac{|v|^2}{4}t)}$, $v \in \mathbb{R}^d$.

Applying the Galilean transform to the solution $e^{it\omega} Q_\omega(x)$ of the NLS on \mathbb{R}^d , we obtain a *soliton* solution, moving on the line $x = tv$ with a velocity $v \in \mathbb{R}^d$:

$$u(t, x) = e^{i(\frac{1}{2}x \cdot v - \frac{1}{4}|v|^2 t + t\omega)} Q_\omega(x - tv). \quad (1.4)$$

The soliton solution is a global solution of the focusing NLS equation, but it is *not* a soliton solution for the NLS_Ω equation: this soliton solution does not satisfy the Dirichlet boundary conditions.

In [32], the first author constructed a solitary wave solution for the $3d$ focusing L^2 -supercritical NLS_Ω equation for large t , which behaves asymptotically as a soliton on the Euclidean space \mathbb{R}^3 , traveling with a velocity v , and moving away from the obstacle. Indeed, let $T_0 > 0$, $c_\omega > 0$ and let Ψ be a C^∞ function such that $\Psi = 0$ near the obstacle and $\Psi = 1$ for $|x| \gg 1$, then

$$\left\| u(t, x) - e^{i(\frac{1}{2}(x \cdot v) - \frac{1}{4}|v|^2 t + t\omega)} Q_\omega(x - tv) \Psi(x) \right\|_{H_0^1(\Omega)} \leq e^{-c_\omega |v| t} \quad \forall (t, x) \in [T_0, +\infty) \times \Omega,$$

is a solution of the NLS_Ω equation. This solution is global in time, however, it does not scatter. For an arbitrary small velocity, this solution proves the optimality of the following threshold for the global existence and scattering given in [28] for the cubic NLS_Ω equation, in dimension $d = 3$: let $u_0 \in H_0^1(\Omega)$ satisfy

$$E_\Omega[u_0] M_\Omega[u_0] < E_{\mathbb{R}^3}[Q] M_{\mathbb{R}^3}[Q], \quad (1.5)$$

$$\|u_0\|_{L^2(\Omega)} \|\nabla u_0\|_{L^2(\Omega)} < \|Q\|_{L^2(\mathbb{R}^3)} \|\nabla Q\|_{L^2(\mathbb{R}^3)}. \quad (1.6)$$

Then the solution $u(t)$ scatters in $H_0^1(\Omega)$ in both time directions.

This threshold was first proved for the $3d$ cubic NLS equation on the whole space \mathbb{R}^3 by the second author with Holmer in [21] (in the radial setting) and with Duyckaerts and Holmer in [14] (nonradial case); further generalizations can be found in [17], [19].

In [15], the first two authors with Duyckaerts studied the dynamics of the focusing $3d$ cubic NLS_Ω equation in the exterior of a strictly convex obstacle at the mass-energy threshold, namely, when

$$E_\Omega[u_0] M_\Omega[u_0] = E_{\mathbb{R}^3}[Q] M_{\mathbb{R}^3}[Q],$$

with the initial mass-gradient bound on $u_0 \in H_0^1(\Omega)$,

$$\|u_0\|_{L^2(\Omega)} \|\nabla u_0\|_{L^2(\Omega)} < \|Q\|_{L^2(\mathbb{R}^3)} \|\nabla Q\|_{L^2(\mathbb{R}^3)},$$

where Q is the ground state solution of (1.3), with $\omega = 1$. The same problem was studied in the whole Euclidean space by Duyckaerts and the second author in [16] for the focusing cubic NLS equation on \mathbb{R}^3 . The dynamics of the NLS equation on the whole Euclidean space is more involved. Indeed, the authors proved that if the initial datum $u_0 \in H^1(\mathbb{R}^3)$ satisfies the same mass-gradient condition as above, then the

solution $u(t)$ scatters or $u(t)$ is a “special solution” Q^+ , up to symmetries, that scatters in negative time and converges to the soliton $e^{it}Q$ (up to symmetries) in positive time. We showed in [15] that this special solution does not have an analogue for the problem in the exterior of an obstacle and prove that such solutions are globally defined and scatter in the positive time direction. The existence of blow-up solutions at the mass-energy threshold for the NLS equation on the whole space was also proved in [16] and the behavior of solutions is related to another special solution Q^- . It was proved that if $E_{\mathbb{R}^3}[u_0]M_{\mathbb{R}^3}[u_0] = E_{\mathbb{R}^3}[Q]M_{\mathbb{R}^3}[Q]$ and $\|u_0\|_{L^2(\mathbb{R}^3)} \|\nabla u_0\|_{L^2(\mathbb{R}^3)} > \|Q\|_{L^2(\mathbb{R}^3)} \|\nabla Q\|_{L^2(\mathbb{R}^3)}$, then the solution $u(t)$ blows up in finite time or $u(t)$ is a special solution Q^- , up to symmetries. The existence of blow-up solutions at the mass-energy threshold $E_{\Omega}[u_0]M_{\Omega}[u_0] = E_{\mathbb{R}^3}[Q]M_{\mathbb{R}^3}[Q]$ and $\|u_0\|_{L^2(\Omega)} \|\nabla u_0\|_{L^2(\Omega)} > \|Q\|_{L^2(\mathbb{R}^3)} \|\nabla Q\|_{L^2(\mathbb{R}^3)}$, for the NLS $_{\Omega}$ equation is currently an open question.

All results obtained for the NLS $_{\Omega}$ equation are for the globally existing and scattering solutions, however, the existence of blow-up solutions has been an open question for some time. The classical proof by the convexity argument on the Euclidean space \mathbb{R}^d fails in the exterior of an obstacle due to the appearance of the boundary terms with an unfavorable sign in the second derivative of the variance $V(u(t))$, that is, if

$$V(u(t)) := \int_{\mathbb{R}^d} |x|^2 |u(t, x)|^2 dx, \quad (1.7)$$

then

$$\frac{1}{16} \frac{d^2}{dt^2} V(u(t)) = E[u] - \frac{1}{2} \left(\frac{d}{2} - \frac{d+2}{p+1} \right) \int_{\Omega} |u|^{p+1} dx - \frac{1}{4} \int_{\partial\Omega} |\nabla u|^2 (x \cdot \vec{n}) d\sigma(x), \quad (1.8)$$

where \vec{n} is the unit outward normal vector. One can see that in the last term

$$x \cdot \vec{n} \leq 0, \text{ for all } x \in \partial\Omega.$$

Recently, the first author in [31] (see also [30]) proved the existence of blow-up solution to the NLS $_{\Omega}$ equation in the exterior of a smooth, compact, convex obstacle. This was the first step in the study of the existence of blow-up solutions to the NLS $_{\Omega}$ equation. A new modified variance $\mathcal{V}(u(t))$, which is bounded from below and is strictly concave for the solutions considered, was introduced

$$\mathcal{V}(u(t)) := \int_{\Omega} \left(d(x, \Omega^c) + 10 \right)^2 |u(t, x)|^2 dx, \quad (1.9)$$

where $d(x, \Omega^c) = |x| - R$ is the distance to the obstacle and R is the radius of the obstacle (a ball in \mathbb{R}^d). In [31] (see also [30]), it was shown that solutions with finite variance and negative energy blow up in finite time (for a ball and also any smooth, compact and convex obstacle). Furthermore, it was proved that finite variance solutions to the NLS $_{\Omega}$ equation for $p \geq 1 + \frac{4}{d}$, which satisfy (1.5), $\|u_0\|_{L^2(\Omega)} \|\nabla u_0\|_{L^2(\Omega)} > \|Q\|_{L^2(\mathbb{R}^3)} \|\nabla Q\|_{L^2(\mathbb{R}^3)}$ and a certain symmetry condition, will blow up in finite time.

From the above review one notices that an obstacle does influence the behavior of solutions and while some properties and criteria remain robust and almost unchanged (except for the restriction of the whole space to the exterior domain problem Ω), other properties either get significantly modified or even more, become unclear in the obstacle setting. Further analytical investigations of the interaction between solutions and an obstacle are needed, though the presence of the obstacle breaks down quite a few invariance properties of the equation, creating additional difficulties for theoretical study.

The purpose of this paper is to investigate this question numerically and to gain further insights of the obstacle influence. We are specifically interested in how solitary wave-type data (e.g., as in (1.4)) interacts with an obstacle, depending on the distance and the angle to the obstacle as well as the size of the obstacle.

In our simulations, we distinguish two types of interaction between a solitary wave solution moving on the line $\vec{x} = t\vec{v}$ (\vec{v} is the velocity vector) and the obstacle:

Strong interaction: We call the interaction *strong*, when a soliton-type solution is moving, towards the obstacle, in the same direction as the outward normal \vec{n} vector of the obstacle, i.e., the velocity vector is collinear to the normal vector, $\vec{v} = \alpha\vec{n}$, $\alpha > 0$, (e.g., see Figure 28). In this case, after the collision or the shock, the solitary wave solution does not preserve the shape of the initial or the original soliton but the solution splits into several solitons or bumps, with a substantial amount of backward reflected waves.

Weak interaction: We call the interaction *weak*, when the velocity vector of the moving soliton solution, towards the obstacle, is not pointed in the same direction as the outward normal vector, i.e., the solution hits the obstacle at an angle $0 < \theta \leq \frac{\pi}{2}$ between the velocity vector and the outward normal vector, see Figure 15. In this case, after the interaction, the solitary wave solution is transmitted almost with the same shape and with backward reflected waves of insignificant size.

The interaction between a solitary wave-type solution and an obstacle does not depend only on the direction of the velocity vector and the angle of the collision, it also depends on the initial distance between the solitary wave solution and the obstacle. For that, we also study the dependence on the distance. Throughout this paper, we denote by

$$d^* := \min_{x \in \text{supp}(u_0)} \text{dist}(x, \Omega^c), \quad (1.10)$$

the distance between the obstacle Ω^c and the essential support of the initial data u_0 such that u_0 is well-defined, i.e., u_0 is smooth and satisfies Dirichlet boundary conditions. Note that, if we consider the initial condition with the distance $d \gg d^*$, then the presence of the obstacle does not effectively influence the behavior of the solution (provided that u_0 has essentially a compact support, for instance, the Gaussian $u_0 = Ae^{-x^2}$ will suffice for computational purposes). If we consider u_0 with a large mass such that $d \gg d^*$, then the solution will blow-up in finite time before it could reach the obstacle for all velocity directions, see Figures 8 and 10 for such scenarios, in such a case, there is no interaction between the obstacle and the solution. Moreover, the computation of the boundary value terms in (1.8) vanishes to 0 when $d \gg d^*$, and one can see that the expression of the second derivative of the variance $V(t)$ in (1.8) is close to the corresponding value of the variance defined on the whole space \mathbb{R}^2 . In this case, numerically, the soliton-type solution behaves as a solution posed on a computational domain without an obstacle, see Figures 4 and 3.

For the purpose of this work, and in order to study the influence and the interaction of a generic solution (a solitary wave-type solution) with an obstacle, we always consider the distance d to be the minimal distance d^* such that even a slight modification of the velocity direction or the translation parameters would produce at least a weak interaction.

In this paper we present our numerical results about the behavior of solutions influenced by an obstacle in the NLS $_{\Omega}$ equation outside of a ball or a disk of radius r_* , in dimension $d = 2$. Our goal is to understand the *interaction* between a solitary wave (for example, traveling with a velocity v) and the obstacle, as well as the *influence* of the obstacle on the nonlinear dynamics of the NLS $_{\Omega}$ equation. We also study the existence of blow-up solutions to the NLS $_{\Omega}$ equation, in dimension $d = 2$, in particular, we investigate the influence of the obstacle on the *behavior* of finite time blow-up solutions, and its dependence on different types of interaction, which is affected by the direction of the velocity v and the angle at the collision. According to our numerical simulations, the solitary wave amplitudes decrease at the collision or at any interaction (even small) between the soliton and the obstacle. This could be explained by the appearance of reflection, or reflection waves,

due to the Dirichlet boundary conditions at the obstacle. After the collision, our numerical results show that, if there is a weak or small interaction, then the solitary wave is transmitted almost completely with little or insignificant backward reflection. If there is a strong interaction, then the solution does not typically preserve the shape of the original solitary wave. First, a single bump will split into two bumps with some substantial backward reflection. After that, the two bumps will start to merge together with a creation of a third bump in the middle and then all of that will continue as a sum of several solitary waves. Typically, the first two bumps will have a dispersive behavior due to a creation of the third middle bump, which will be the main part of the (after-interaction) solitary wave.

We also observe that the leading reflected wave has a dispersive behavior, which radiates away. The reflection phenomenon, the loss of the amplitude and the change in the shape of the solitary wave, make it very challenging to show (even numerically) the existence of blow-up solutions. Nevertheless, we confirm numerically the existence of blow-up solutions *after the collision* for the $2d$ focusing NLS $_{\Omega}$ equation in several cases of: (i) the weak interaction, depending on the velocity direction, see Section 6; (ii) the strong interaction, depending on the radius r_{\star} of the obstacle. Moreover, we investigate the influence of the size of the obstacle on the behavior of the solutions in terms of the transmitted and reflected mass: (i) if the radius of the obstacle is very small (e.g., $r_{\star} \approx 0.1$), so that the interaction region of the solution with the obstacle is insignificant or negligible, then the solution is mostly transmitted with a small reflected part and it blows up in finite time after the interaction; (ii) if the radius of the obstacle is large enough, so that the interaction region is relevant and it is larger than the contour of the solution (e.g., $r_{\star} \approx 2$), then there is almost no transmission of the solution and it blows up in finite time at the boundary of the obstacle, see Section 8. Furthermore, we construct new *Wall-type* initial data (with a single maximum peak bump), where after a strong interaction with the obstacle, the corresponding solutions blow up in finite time in two different locations (this happens even for a larger obstacle size). These specific solutions to the NLS $_{\Omega}$ equation have a very distinct dynamics compared with all other blow-up scenarios and dynamics we observed, since they can produce a blow up not at a single location, see Section 9; there is also interesting dynamics for certain parameters when the blow-up happens at a single point after the strong interaction (Figure 43).

In addition, we study the *sharp threshold* for global existence vs. finite time blow-up solutions (in the $2d$ focusing mass-critical NLS $_{\Omega}$ equation), see Section 4. This threshold was first obtained by Weinstein in [47] for the focusing mass-critical NLS equation in the whole Euclidean space \mathbb{R}^d (for example, $2d$ cubic NLS). He showed a sharp threshold for the global existence using the Gagliardo-Nirenberg inequality combined with the energy conservation,

$$\|\nabla u\|_{L^2}^2 \leq \left(1 - \frac{\|u\|_{L^2}^2}{\|Q\|_{L^2}^2}\right)^{-1} E[u],$$

which implies that (i) if $\|u_0\|_{L^2} < \|Q\|_{L^2}$, then an H^1 solution exists globally in time and (ii) if $\|u_0\|_{L^2} \geq \|Q\|_{L^2}$, then the solution may blow up in finite time. Recently, Dodson proved in [13] that initial data $u_0 \in L^2(\mathbb{R}^d)$ with $\|u_0\|_{L^2} < \|Q\|_{L^2}$ generates a corresponding solution that is global and scatters in $L^2(\mathbb{R}^d)$. To confirm this threshold in our setting of the NLS with an obstacle, we consider initial data u_0 as a small perturbation of a shifted soliton, $u_0 = A Q(x - x_0)$, with either $A < 1$ (e.g. $A = 0.9$) for global existence or $A > 1$ (e.g., $A = 1.1$) for a finite time of existence.

In physics, the study of the reflected, diffracted or scattered (mechanical, electromagnetic or gravitational) waves after encountering an object, an obstacle or a body, is related to the study of boundary value problems. These problems are usually described mathematically as an exterior domain or obstacle problem for the wave-type equations with Dirichlet or Neuman boundary conditions. The study of the wave-type equations in the exterior of an obstacle started in the late 1950s and early 1960s and until now the understanding of the dynamics of the evolution equations on exterior domains has been a widely open area for investigations.

Let us mention, some relevant works on the wave-type equation in an exterior domain. H. W. Calvin and Morawetz have studied the local-energy decay of the solutions to the linear wave equation in an exterior of a sphere and star-shape obstacles, with Dirichlet and Neuman boundary conditions, see [48] and [35], [36]. For later works see [33], [34]. Different results were obtained for almost-star shape, non-trapping and moving obstacles, see [25], [37], [38] and [11]. In that period of time, the authors considered a classical solutions with C^2 initial data. In 2004, the Cauchy theory in $H_0^1(\Omega)$ for the NLS_Ω equation was initiated by Burq, Gérard and Tzvetkov in [9], for a non-trapping obstacle. After that, the well-posedness problem for the NLS_Ω equation was investigated by others, see for example, [3], [24], [42], [23], [8]. In [32], the first author proved the local well-posedness for the $3d$ NLS_Ω equation in the critical Sobolev space using the fractional chain rule in the exterior of a compact convex obstacle given in [27].

This paper is organized as follows: in Section 2 we present the numerical method that we design for this study. In Section 3, we show several numerical simulations of scattering and blow-up solutions for the focusing nonlinear Schrödinger equation on the whole Euclidean space \mathbb{R}^2 for later comparison. In Section 4, we study the sharp threshold for global existence and blow-up solutions for the critical NLS_Ω equation in terms of the ground state perturbations. In Section 5, we fix the radius r_\star of the obstacle (e.g., $r_\star = 0.5$) and study the dependence of the interaction on the initial distance between the solution and the obstacle, depending on the velocity direction. In Sections 6 and 7, we study the weak and strong interactions between the traveling solutions and the obstacle. In Section 8, we investigate the influence of the size of the obstacle r_\star on the behavior of solutions, especially in the strong interaction case. Finally, in Section 9, we study the existence of blow-up solutions, with the new *Wall-type* initial data, for a variety of large size obstacles and different initial amplitude of the data. We summarize our findings in conclusions' Section 10. In all our simulations we consider both the cubic (mass-critical) and quintic (mass-supercritical) NLS_Ω equations.

Acknowledgments. All authors would like to thank Thomas Duyckaerts for fruitful discussions on this problem. Most of the research on this project was done while O.L. was visiting the Department of Mathematics and Statistics at Florida International University, Miami, FL, during his PhD training. He thanks the department for hospitality and support. The initial numerical investigations started when K.Y. visited T. Duyckaerts at IHP and LAGA, Paris-13. S.R. and K.Y. were partially supported by the NSF grant DMS-1927258, and part of O.L.'s research visit to FIU was funded by the same grant DMS-1927258 (PI: Roudenko).

2. NUMERICAL APPROACH

2.1. The scheme and Initial data. Various numerical methods are used in order to approximate the non-linear Schrödinger equation ranging from the explicit and implicit schemes in time to the finite difference or Fourier pseudo-spectral methods in space. There are different methods for the time discretization, for example, the Crank-Nicolson scheme [12], Runge-Kutte type [1], [2], [26], symplectic and splitting type, [45], [44] and [46], [7] and relaxation methods [5] and [6].

We use the well-known Crank-Nicolson scheme for the time discretization of the NLS_Ω equation. The scheme is based on a time centering approximation $u^{n+\frac{1}{2}} \approx \frac{u^{n+1}+u^n}{2}$. The Crank-Nicolson-type scheme is the 2nd order implicit method. On the plus side, this scheme preserves both the discrete mass and the discrete energy exactly during the time evolution. On the negative side, the schemes have to deal with solving the resulting *nonlinear* algebraic system, consequently, the Newton's iterative method (2.5) is used for solving the nonlinear system at each time step.

We consider exponentially decaying data only and we take a large enough computational domain to approximate the convex domain Ω containing an obstacle (of radius r_*). To be specific, we consider the polar coordinates (r, θ) with $0 < r_* < r < R$ and $0 \leq \theta \leq 2\pi$ and use the following domain in our simulations:

$$\Omega = \{(r, \theta) \in \mathbb{R}^2 : r_* \leq r \leq R, 0 \leq \theta \leq 2\pi\}.$$

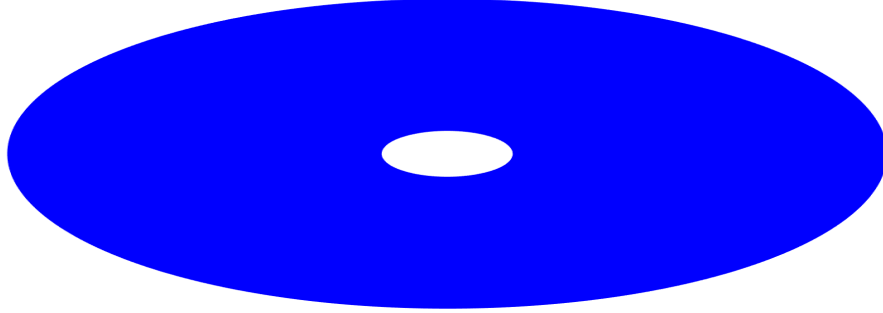


FIGURE 1. The computational domain Ω .

The obstacle is the white region or the disk $[0, r_*] \times [0, 2\pi]$, see Figure 1. We note that the obstacle size is fixed as $r_* = 0.5$, unless stated otherwise, for example, a variable parameter or an investigating variable in Sections 8 and 9.

It is straightforward to see that to approximate our model, we need to impose the Dirichlet boundary condition on the variable r , i.e., $u(r_*, \theta, t) = u(R, \theta, t) = 0$, and the periodic boundary conditions on the variable θ , i.e., $u(r, 0, t) = u(r, 2\pi, t)$.

Initial data : We consider the following initial data,

$$u_0(r, \theta) = A_0 F(r \cos \theta - x_c, r \sin \theta - y_c) e^{i \frac{1}{2}(v_x \cdot r \cos \theta + v_y \cdot r \sin \theta)}, \quad (2.1)$$

where A_0 is the initial amplitude, (x_c, y_c) is the translation, $v = (v_x, v_y)$ is the velocity vector, and F is the profile of the solutions, which is typically taken as the Gaussian; for example, $F = e^{-r^2/2}$. To be precise, we consider

$$u_0(r, \theta) = A_0 e^{-\frac{1}{2}[(r \cos \theta - x_c)^2 + (r \sin \theta - y_c)^2]} e^{i \frac{1}{2}(v_x \cdot r \cos \theta + v_y \cdot r \sin \theta)}. \quad (2.2)$$

Throughout the paper, in most cases we use the same Gaussian initial data (2.2), (unless indicated otherwise as in Sections 4 and 9). The amplitude, translation and velocity parameters vary according to the specific examples considered.

We next describe our algorithm. We first consider the time discretization. Let T_{max} be the existence time of the solution and $T_{\Delta t}$ be the computational time ($T_{\Delta t} < T_{max}$). We use N points for the time discretization, thus, defining a time step $\Delta t = \frac{T_{\Delta t}}{N}$. We discretize the NLS $_{\Omega}$ equation at times $t_n = n\Delta t$, $n = 0, \dots, N$, by considering the semi-discretization in time $u^n \approx u(x, t_n)$ with $u^0 := u_0$. This yields the following time evolution:

$$i \frac{u^{n+1} - u^n}{\Delta t} + \frac{1}{2} \Delta u^{n+1} + \frac{1}{2} \Delta u^n = -F(u^{n+1}, u^n), \quad (2.3)$$

where F is the nonlinear term $|u|^{p-1}u$ approximated by

$$F(u^{n+1}, u^n) := \frac{2}{p+1} \frac{|u^{n+1}|^{p+1} - |u^n|^{p+1}}{|u^{n+1}|^2 - |u^n|^2} \frac{u^{n+1} + u^n}{2}. \quad (2.4)$$

Note that, u^n is the known variable and for $n = 0$, $u^0 = u_0$ is the given initial condition. We compute the evolution $u^n \rightarrow u^{n+1}$ by solving the above system (2.3). For that, we use the Newton iteration to solve the nonlinear implicit system (2.3). We denote u^{n+1} at the iteration l by $u^{n+1,l}$ and assume $u^{n+1} = u^{n+1,\infty}$, which gives

$$\begin{cases} u^{n+1,l+1} = u^{n+1,l} - J^{-1} \cdot G(u^{n+1,l}), \\ u^{n+1,0} = 1.001 \cdot u^n, \end{cases} \quad (2.5)$$

where $G(u^{n+1}) = u^{n+1} - u^n + \frac{\Delta t}{2i} \Delta u^{n+1} + \frac{\Delta t}{2i} \Delta u^n + F(u^{n+1}, u^n)$ and J is the Jacobian of G .

The stopping criterion for (2.5) is $\|u^{n+1,l+1} - u^{n+1,l}\|_{L^\infty} < Tol$ for some small constant Tol . In our simulation, we take $Tol < 10^{-13}$, which is close to the machine precision. In order to reach the blow-up time (or the closest time), we slightly decrease the tolerance according to the examples treated.

We employ the polar transformation in space $x = r \cos \theta$ and $y = r \sin \theta$ to convert the problem into the polar coordinate setting. Thus, we write the Laplacian in polar coordinates as

$$\Delta u(r, \theta) = \frac{\partial}{\partial r} \left(r \frac{\partial}{\partial r} u(r, \theta) \right) + \frac{1}{r^2} \frac{\partial^2}{\partial \theta^2} u(r, \theta), \quad (r, \theta) \in \Omega. \quad (2.6)$$

We then rewrite the NLS $_\Omega$ equations for $t \in (0, T)$, $(r, \theta) \in \Omega$, as

$$i \frac{\partial}{\partial t} u(t, r, \theta) + \frac{\partial}{\partial r} \left(r \frac{\partial}{\partial r} u(t, r, \theta) \right) + \frac{1}{r^2} \frac{\partial^2}{\partial \theta^2} u(t, r, \theta) = -|u(t, r, \theta)|^{p-1} u(t, r, \theta)$$

with the periodic boundary condition on θ

$$u(t, r, 0) = u(t, r, 2\pi), \quad \forall t \in [0, T], \forall r \in [r_\star, R], \quad (2.7)$$

and the Dirichlet boundary condition on r

$$u(t, r_\star, \theta) = u(t, R, \theta) = 0, \quad \forall t \in [0, T], \forall \theta \in [0, 2\pi]. \quad (2.8)$$

We use N_r and N_θ to denote the number of points for the space discretization, setting

$$\Delta r = \frac{R - r_\star}{N_r} \quad \text{and} \quad \Delta \theta = \frac{2\pi}{N_\theta}.$$

We denote the full discretization by $u_{k,j}^n \approx u(r_k, \theta_j, t_n)$, $r_k = r_\star + k\Delta r$, $\theta_j = j\Delta \theta$, for $n = 0, \dots, N$, $k = 0, \dots, N_r$ and $j = 0, \dots, N_\theta$.

We use the second order finite difference scheme in space, to approximate the NLS $_\Omega$ equation:

$$i \frac{u_{k,j}^{n+1} - u_{k,j}^n}{\Delta t} + \frac{1}{2} [D_r + D_\theta] u_{k,j}^{n+1} + \frac{1}{2} [D_r + D_\theta] u_{k,j}^n = -F(u_{k,j}^{n+1}, u_{k,j}^n), \quad (2.9)$$

where $F(u_{k,j}^{n+1}, u_{k,j}^n)$ is defined in (2.4) and

$$D_r u_{k,j}^n = \frac{1}{\Delta r} \frac{1}{r_k} \left(r_{k+\frac{1}{2}} \frac{u_{k+1,j}^n - u_{k,j}^n}{\Delta r} - r_{k-\frac{1}{2}} \frac{u_{k,j}^n - u_{k-1,j}^n}{\Delta r} \right), \quad (2.10)$$

$$D_\theta u_{k,j}^n = \frac{1}{r_k^2} \frac{u_{k,j+1}^n - 2u_{k,j}^n + u_{k,j-1}^n}{(\Delta \theta)^2}, \quad (2.11)$$

$$F(u_{k,j}^{n+1}, u_{k,j}^n) = \frac{2}{p+1} \frac{|u_{k,j}^{n+1}|^{p+1} - |u_{k,j}^n|^{p+1}}{|u_{k,j}^{n+1}|^2 - |u_{k,j}^n|^2} \frac{u_{k,j}^{n+1} + u_{k,j}^n}{2}, \quad (2.12)$$

where $r_{k+\frac{1}{2}} = \frac{r_k + r_{k+1}}{2}$, and using the convention that $u_{0,j}^n = u_{N_r,j}^n = 0$, $u_{k,0}^n = u_{k,N_\theta}^n$ and $u_{k,1}^n = u_{k,N_\theta+1}^n$ from the boundary settings.

To solve the above system (2.9) with (2.10) and (2.11), we consider the initial condition such that u_0 satisfies Dirichlet boundary conditions. We typically consider a shifted Gaussian as an initial condition,

therefore, we define the translation parameters (x_c, y_c) such that u_0 is smooth and vanishes to 0 near both the obstacle and the boundary of the computational domain.

2.2. Mass and Energy conservation. The Crank-Nicolson scheme (2.3) conserves the following discretized quantities: the discretized L^2 -norm, or often referred to as the *discrete* mass, and the discretized energy, called the *discrete* energy, which are the discrete analogues of the mass and energy conservations in (1.1) and (1.2).

If we consider the rectangular coordinates (x, y) , and the discretization of the Laplacian term Δu by the standard five points stencil finite difference approximation (e.g., see [12]), i.e.,

$$\Delta u_{k,j} \approx \frac{u_{k-1,j} + u_{k+1,j} + u_{k,j-1} + u_{k,j+1} - 4u_{k,j}}{\Delta x \Delta y}, \quad (2.13)$$

by assuming $\Delta x = x_{k+1} - x_k = \Delta y$, then the conservation of the discrete mass for the scheme (2.3) with the Laplacian Δu approximated by (2.13) on the rectangular domain is given by

$$M[u^n] = \sum_{k=0}^{N_x} \sum_{j=0}^{N_y} |u_{k,j}^n|^2 \Delta x \Delta y = M[u^0], \quad \text{for } n \geq 0, \quad (2.14)$$

which can be proved by multiplying the equation (2.3) by $(\bar{u}_{k,j}^{n+1} + \bar{u}_{k,j}^n) \Delta x \Delta y$ and summing from $k = 0$ to N_x , and $j = 0$ to N_y for each k, j .

Similarly, the conservation of the discrete energy in rectangular coordinates (x, y) is obtained by multiplying (2.3) with $(\bar{u}_{k,j}^{n+1} - \bar{u}_{k,j}^n) \Delta x \Delta y$, summing from $k = 0$ to N_x and $j = 0$ to N_y for each k, j and taking the real part:

$$E[u^n] = \frac{1}{2} \sum_{k=0}^{N_x-1} \sum_{j=0}^{N_y-1} \left(\left| \frac{u_{k+1,j}^n - u_{k,j}^n}{\Delta x} \right|^2 + \left| \frac{u_{k,j+1}^n - u_{k,j}^n}{\Delta y} \right|^2 - \frac{2}{p+1} |u_{k,j}^n|^{p+1} \right) \Delta x \Delta y = E[u_0], \quad \text{for } n \geq 0. \quad (2.15)$$

For brevity, we omit the above standard proofs.

In polar coordinates (r, θ) , the scheme (2.9) also conserves the discrete mass and energy exactly, similarly to the above. More specifically, we define the discrete mass at $t = t_n$ by

$$M[u^n] = \sum_{k=0}^{N_r} \sum_{j=0}^{N_\theta} |u_{k,j}^n|^2 r_k \Delta r \Delta \theta, \quad \text{for } n \geq 0. \quad (2.16)$$

One can see that the definition (2.16) is an analog to the mass in (1.1). In the same spirit, we define the discrete energy as

$$E[u^n] = \frac{1}{2} \sum_{k=0}^{N_r} \sum_{j=0}^{N_\theta} \left(\left| \frac{u_{k+1,j}^n - u_{k,j}^n}{\Delta r} \right|^2 r_{k+\frac{1}{2}} \Delta r \Delta \theta + \frac{1}{2} \frac{1}{r_k} \left| \frac{u_{k,j+1}^n - u_{k,j}^n}{\Delta \theta} \right|^2 \Delta r \Delta \theta \right) - \frac{1}{p+1} \sum_{k=0}^{N_r} \sum_{j=0}^{N_\theta} |u_{k,j}^n|^{p+1} r_k \Delta r \Delta \theta, \quad \text{for } n \geq 0, \quad (2.17)$$

which is an analog of the energy conservation in (1.2).

We have the following theorem:

Theorem A. *The numerical scheme (2.9) conserves the discrete mass (2.16) and the discrete energy (2.17) for all $n \in \mathbb{N}$, i.e.,*

$$M[u^n] = M[u_0] \quad \text{and} \quad E[u^n] = E[u_0].$$

Proof. The proof of the mass conservation is similar to the proof in the case of the rectangular coordinates (x, y) , it suffices to multiply (2.9) with $(\bar{u}_{k,j}^{n+1} + \bar{u}_{k,j}^n) r_k \Delta r \Delta \theta$, sum up over k and j from 0 to N_r , 0 to N_θ , respectively, and then take the imaginary part.

For the energy-conservation, the proof is slightly different than the one in the rectangular coordinates (x, y) , due to the space discretization of the Laplacian in (2.10). For that, we write the scheme (2.9) for $u_{k,j}^n$, using (2.10), (2.11) and (2.12), to obtain

$$\begin{aligned}
& \underbrace{i \frac{u_{k,j}^{n+1} - u_{k,j}^n}{\Delta t}}_{(I_1)_{k,j}} + \underbrace{\frac{1}{2} \frac{1}{r_k} \frac{1}{\Delta r} \left(r_{k+\frac{1}{2}} \frac{u_{k+1,j}^{n+1} - u_{k+1,j}^n}{\Delta r} - r_{k-\frac{1}{2}} \frac{u_{k,j}^{n+1} - u_{k-1,j}^n}{\Delta r} \right)}_{(I_{2,1})_{k,j}} \\
& + \underbrace{\frac{1}{2} \frac{1}{r_k} \frac{1}{\Delta r} \left(r_{k+\frac{1}{2}} \frac{u_{k+1,j}^n - u_{k,j}^n}{\Delta r} - r_{k-\frac{1}{2}} \frac{u_{k,j}^n - u_{k-1,j}^n}{\Delta r} \right)}_{(I_{2,2})_{k,j}} + \underbrace{\frac{1}{2} \frac{1}{(r_k)^2} \frac{u_{k,j+1}^{n+1} - 2u_{k,j}^{n+1} + u_{k,j-1}^{n+1}}{(\Delta \theta)^2}}_{(I_{3,1})_{k,j}} \\
& + \underbrace{\frac{1}{2} \frac{1}{(r_k)^2} \frac{u_{k,j+1}^n - 2u_{k,j}^n + u_{k,j-1}^n}{(\Delta \theta)^2}}_{(I_{3,2})_{k,j}} = \underbrace{-\frac{1}{p+1} \frac{|u_{k,j}^{n+1}|^{p+1} - |u_{k,j}^n|^{p+1}}{|u_{k,j}^{n+1}|^2 - |u_{k,j}^n|^2} (u_{k,j}^{n+1} + u_{k,j}^n)}_{(I_4)_{k,j}} \quad (2.18)
\end{aligned}$$

Multiplying (2.18) with $(\bar{u}_{k,j}^{n+1} - \bar{u}_{k,j}^n) r_k \Delta r \Delta \theta$, taking the real part and summing up over k and j , yields

$$\operatorname{Re} \left[\sum_{k=0}^{N_r} \sum_{j=0}^{N_\theta} (I_1)_{k,j} \times (\bar{u}_{k,j}^{n+1} - \bar{u}_{k,j}^n) r_k \Delta r \Delta \theta \right] = 0. \quad (2.19)$$

$$\begin{aligned}
\operatorname{Re} \left[\sum_{k=0}^{N_r} \sum_{j=0}^{N_\theta} ((I_{2,1})_{k,j} + (I_{2,2})_{k,j}) \times (\bar{u}_{k,j}^{n+1} - \bar{u}_{k,j}^n) r_k \Delta r \Delta \theta \right] &= \sum_{k=0}^{N_r} \sum_{j=0}^{N_\theta} -\frac{1}{2} r_{k+\frac{1}{2}} \left| \frac{u_{k+1,j}^{n+1} - u_{k-1,j}^{n+1}}{\Delta r} \right|^2 \Delta r \Delta \theta \\
&+ \sum_{k=0}^{N_r} \sum_{j=0}^{N_\theta} \frac{1}{2} r_{k+\frac{1}{2}} \left| \frac{u_{k+1,j}^n - u_{k,j}^n}{\Delta r} \right|^2 \Delta r \Delta \theta. \quad (2.20)
\end{aligned}$$

Using that $\bar{u}_{k,N_\theta}^n = \bar{u}_{k,0}^n$, $u_{k,N_\theta+1}^n = u_{k,1}^n$, $u_{k,N_\theta}^n = u_{k,0}^n$ and $u_{0,j}^n = u_{N_r,j}^n = 0$, for all $n \in \mathbb{N}$, we get

$$\begin{aligned}
\operatorname{Re} \left[\sum_{k=0}^{N_r} \sum_{j=0}^{N_\theta} (I_{3,1})_{k,j} \times (\bar{u}_{k,j}^{n+1} - \bar{u}_{k,j}^n) r_k \Delta r \Delta \theta \right] &= -\frac{1}{2} \frac{1}{r_k} \operatorname{Re} \sum_{k=0}^{N_r} \sum_{j=0}^{N_\theta} \left| \frac{u_{k,j}^{n+1} - u_{k,j-1}^{n+1}}{\Delta \theta} \right|^2 \Delta r \Delta \theta \\
&- \frac{1}{2} \frac{1}{r_k} \frac{1}{(\Delta \theta)^2} \operatorname{Re} \left[\sum_{k=0}^{N_r} \sum_{j=0}^{N_\theta} u_{k,j+1}^{n+1} \bar{u}_{k,j}^n + 2u_{k,j}^{n+1} \bar{u}_{k,j}^n - u_{k,j-1}^{n+1} \bar{u}_{k,j}^n \right] \Delta r \Delta \theta. \quad (2.21)
\end{aligned}$$

Similarly, we deduce

$$\begin{aligned}
\operatorname{Re} \left[\sum_{k=0}^{N_r} \sum_{j=0}^{N_\theta} (I_{3,2})_{k,j} \times (\bar{u}_{k,j}^{n+1} - \bar{u}_{k,j}^n) r_k \Delta r \Delta \theta \right] &= \frac{1}{2} \frac{1}{r_k} \operatorname{Re} \sum_{k=0}^{N_r} \sum_{j=0}^{N_\theta} \left| \frac{u_{k,j}^n - u_{k,j-1}^n}{\Delta \theta} \right|^2 \Delta r \Delta \theta \\
&- \frac{1}{2} \frac{1}{r_k} \frac{1}{(\Delta \theta)^2} \operatorname{Re} \sum_{k=0}^{N_r} \sum_{j=0}^{N_\theta} \left[-\bar{u}_{k,j+1}^{n+1} u_{k,j}^n - 2\bar{u}_{k,j}^{n+1} u_{k,j}^n + \bar{u}_{k,j-1}^{n+1} u_{k,j}^n \right] \Delta r \Delta \theta. \quad (2.22)
\end{aligned}$$

By (2.22) and (2.21), we obtain

$$\begin{aligned} \operatorname{Re} \left[\sum_{k=0}^{N_r} \sum_{j=0}^{N_\theta} ((I_{3,1})_{k,j} + (I_{3,2})_{k,j}) \times (\bar{u}_{k,j}^{n+1} - \bar{u}_{k,j}^n) r_k \Delta r \Delta \theta \right] &= -\frac{1}{2} \frac{1}{r_k} \operatorname{Re} \sum_{k=0}^{N_r} \sum_{j=0}^{N_\theta} \left| \frac{u_{k,j}^{n+1} - u_{k,j-1}^{n+1}}{\Delta \theta} \right|^2 \Delta r \Delta \theta \\ &\quad + \frac{1}{2} \frac{1}{r_k} \operatorname{Re} \sum_{k=0}^{N_r} \sum_{j=0}^{N_\theta} \left| \frac{u_{k,j}^n - u_{k,j-1}^n}{\Delta \theta} \right|^2 \Delta r \Delta \theta, \end{aligned} \quad (2.23)$$

$$\operatorname{Re} \left[\sum_{k=0}^{N_r} \sum_{j=0}^{N_\theta} (I_4)_{k,j} \times (\bar{u}_{k,j}^{n+1} - \bar{u}_{k,j}^n) r_k \Delta r \Delta \theta \right] = -\frac{1}{p+1} \sum_{k=0}^{N_r} \sum_{j=0}^{N_\theta} (|u_{k,j}^{n+1}|^{p+1} - |u_{k,j}^n|^{p+1}) r_k \Delta r \Delta \theta. \quad (2.24)$$

Summing up (2.19), (2.20), (2.23) and (2.24), we finally arrive at

$$\begin{aligned} E[u^n] &= \frac{1}{2} \sum_{k=0}^{N_r} \sum_{j=0}^{N_\theta} r_{k+\frac{1}{2}} \left| \frac{u_{k+1,j}^n - u_{k,j}^n}{\Delta r} \right|^2 \Delta r \Delta \theta + \frac{1}{2} \frac{1}{r_k} \left| \frac{u_{k,j+1}^n - u_{k,j}^n}{\Delta \theta} \right|^2 \Delta r \Delta \theta \\ &\quad - \frac{1}{p+1} \sum_{k=0}^{N_r} \sum_{j=0}^{N_\theta} |u_{k,j}^n|^{p+1} r_k \Delta r \Delta \theta \\ &= \frac{1}{2} \sum_{k=0}^{N_r} \sum_{j=0}^{N_\theta} r_{k+\frac{1}{2}} \left| \frac{u_{k+1}^{n+1} - u_k^{n+1}}{\Delta r} \right|^2 \Delta r \Delta \theta + \frac{1}{2} \frac{1}{r_k} \left| \frac{u_{k,j+1}^{n+1} - u_{k,j}^{n+1}}{\Delta \theta} \right|^2 \Delta r \Delta \theta \\ &\quad - \frac{1}{p+1} \sum_{k=0}^{N_r} \sum_{j=0}^{N_\theta} |u_{k,j}^{n+1}|^{p+1} r_k \Delta r \Delta \theta = E[u^{n+1}]. \end{aligned}$$

□

We note that in our simulations the mass and the energy are well preserved: the relative mass-error and energy-error are bounded by at least 10^{-14} , at the end of the simulations at $T = 20$ with the time step 10^{-2} , as shown in Figure 2. The evolution of the relative mass and energy errors can be tracked by

$$\max_{0 \leq m \leq n} (M[u^m]) - \min_{0 \leq m \leq n} (M[u^m]) \quad \text{and} \quad \max_{0 \leq m \leq n} (E[u^m]) - \min_{0 \leq m \leq n} (E[u^m]), \quad (2.25)$$

or

$$\frac{M[u^n] - M[u_0]}{M[u_0]} \quad \text{and} \quad \frac{E[u^n] - E[u_0]}{E[u_0]}. \quad (2.26)$$

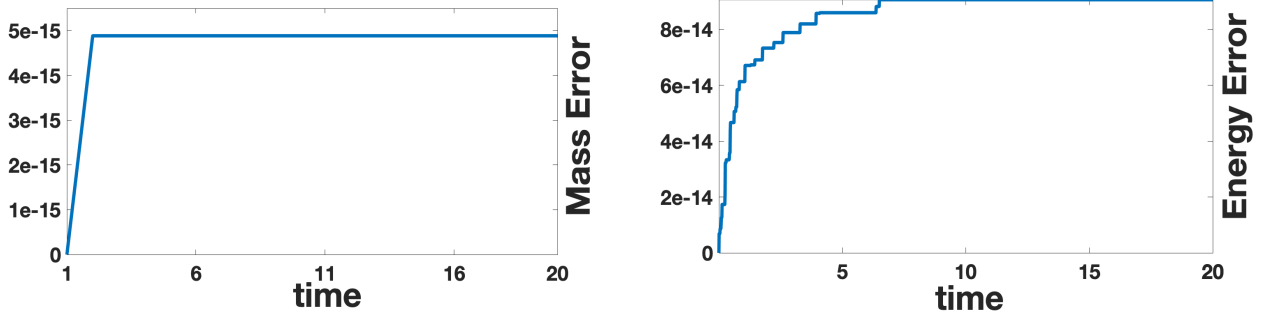


FIGURE 2. Evolution of the relative mass and energy errors (2.25) in the scheme (2.9) for $d = 2$ and $p = 3$.

In Figure 2, we show that the error in (2.25) for the discrete mass and energy are on the order of 10^{-15} and 10^{-14} , correspondingly. The errors of mass and energy in the case for $p = 5$ are on the same order.

3. THE NLS EQUATION ON THE WHOLE PLANE \mathbb{R}^2

In this section, we show different numerical solutions of the focusing nonlinear Schrödinger equation on the whole Euclidean space \mathbb{R}^2 . We give several single bump solitary wave-type examples (and their evolution on the whole \mathbb{R}^2 plane) that we later consider in the following sections when investigating the influence of the obstacle on the behavior of the NLS_Ω solutions with the same initial data for comparison.

Here, we consider a sufficiently large regular bounded rectangular domain without an obstacle and impose the Dirichlet boundary conditions on the boundary. In order to approximate the $NLS_{\mathbb{R}^2}$ equation, the Laplacian term Δu is discretized in the way of (2.13), and the temporal discretization is achieved by the Crank-Nicolson scheme in (2.3), with the Newton's iteration solving the resulting fully discretized nonlinear algebraic system.

3.1. The L^2 -critical case: 2d cubic NLS on \mathbb{R}^2 . We consider the focusing cubic $NLS_{\mathbb{R}^2}$ equation with initial data as in (2.2), moving on the line $y = x$ with the following parameters:

$$A_0 = 2.25, \quad v = (15, 15) \quad \text{and} \quad (x_c, y_c) = (-4.5, -4.5). \quad (3.1)$$

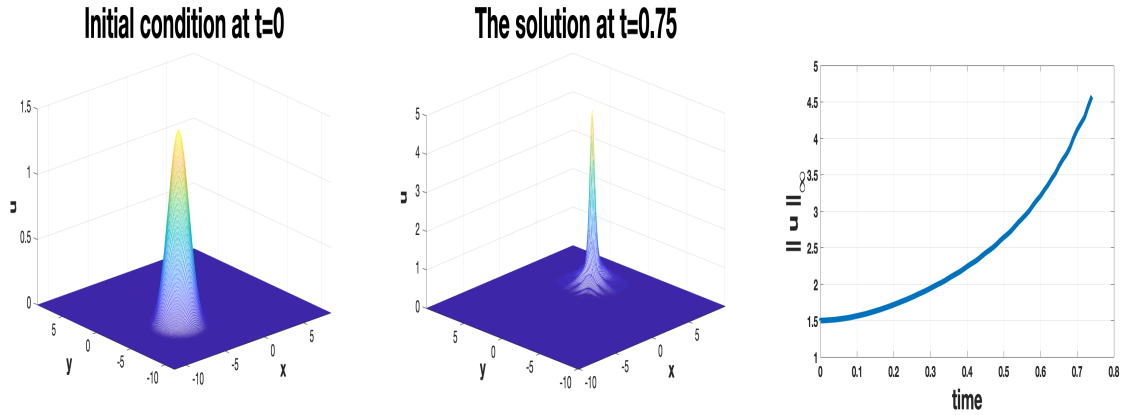


FIGURE 3. Solution to the 2d cubic NLS with initial data u_0 as in (2.2) with $A_0 = 2.25$, $v = (15, 15)$ and $(x_c, y_c) = (-4.5, -4.5)$ at times $t = 0$ and $t = 0.75$ moving along the line $y = x$ (left and middle); time dependence of the L^∞ -norm of this solution (right).

Snapshots of the initial data and the solution $u(t)$ to $NLS_{\mathbb{R}^2}$ equation, which blows up in finite time (shortly after $t = 0.75$), is plotted in Figure 3 on the left ($t = 0$) and middle ($t = 0.75$, the last computational time before the blow-up) subplots. The right subplot is the L^∞ -norm of the solution, which increases toward ∞ , indicating the blow-up. We note that the same initial condition with exactly the same parameters (3.1), will have a different evolution when an obstacle is present, see Figures 25, 26, see also Figures 18, 19, for similar initial condition with $v = (12, 15)$ and $v = (15, 12)$. Note that, in the presence of the obstacle, we also impose Dirichlet boundary condition for the initial data on the obstacle boundary, see (2.8).

3.2. The L^2 -supercritical case: 2d quintic NLS on \mathbb{R}^2 . We consider the focusing quintic $NLS_{\mathbb{R}^2}$ equation with initial data u_0 as in (2.2) with

$$A_0 = 1.25, \quad v = (15, 0) \quad \text{and} \quad (x_c, y_c) = (-4.5, 0).$$

When there is no obstacle present, the solution $u(t)$ to the $NLS_{\mathbb{R}^2}$ equation, which is moving along the line $y = 0$, blows up in finite time slightly after $t = 0.64$, see Figure 4 snapshots of the solution at $t = 0$ and $t = 0.64$ (initial time and the last computational time before the blow-up) on the left and middle subplots and the L^∞ -norm on the right subplot. We observe later that the solution to the NLS_Ω equation with the same initial data, when the obstacle is present, does not blow-up in finite time and has a completely

different dynamics. Furthermore, the solitary wave does not preserve its shape or profile after the collision or interaction with the obstacle (see Figure 29, 30, and Table 2).

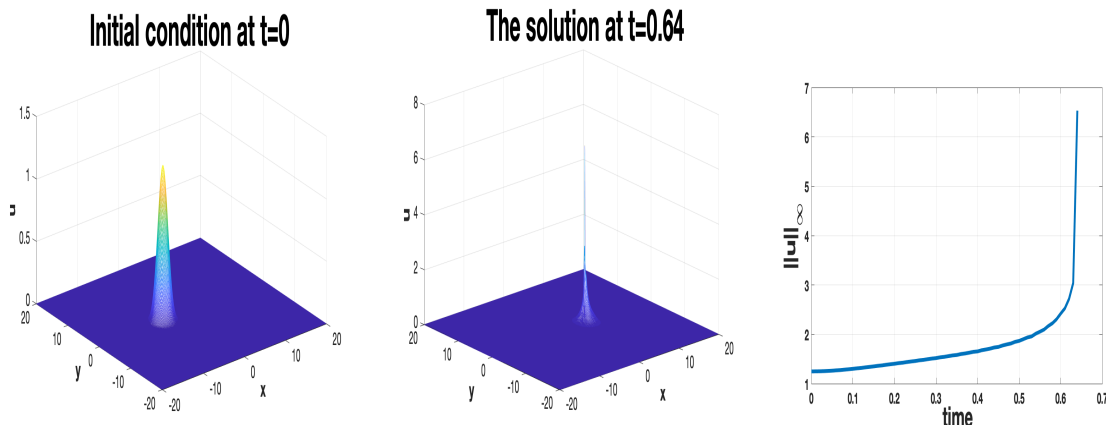


FIGURE 4. Solution to the $2d$ quintic NLS with initial data u_0 as in (2.2) with $A_0 = 1.25$, $v = (15, 0)$ and $(x_c, y_c) = (-4.5, 0)$ at times $t = 0$ and $t = 0.64$ moving on the line $y = 0$ (left and middle); time dependence of the L^∞ -norm of this solution (right).

Let us mention that, for a sufficiently large amplitude A_0 , the solution for the $\text{NLS}_{\mathbb{R}^2}$ equation, considered on the whole Euclidean space \mathbb{R}^2 , blows up in finite time (for more details about thresholds values of A_0 for scattering and blow-up in the focusing NLS, see [20]). We also mention that if A_0 is sufficiently small (for example, in the L^2 -critical case when $\|u_0\|_{L^2} < \|Q\|_{L^2}$, or in the L^2 -supercritical case with initial data under the so-called mass-energy threshold, see for example [21]), then the solution will scatter (in both cases with or without an obstacle), and while there maybe some small reflecting waves formed in the latter (obstacle) case, we omit this case here, and point out reflecting waves later.

4. PERTURBATIONS OF THE SOLITON IN THE NLS WITH OBSTACLE

We now start investigating the $2d$ NLS on the domain with an obstacle, NLS_Ω . In this section we consider a multiple of the ground state that is shifted by (x_c, y_c) as in (2.1), we refer to this evolution as a perturbed soliton, since the initial data have the form

$$u_0(r, \theta) = \lambda Q(r \cos \theta - x_c, r \sin \theta - y_c), \quad \lambda \in \mathbb{R},$$

where Q is the ground state solution to (1.3). This ground state solution is obtained numerically via the Petviashvili's iteration, for example, see [41], [40], [39] or the work of the last two authors in [43] or [49, 50].

Perturbations of the soliton solution to the NLS_Ω equation with a ‘large mass’ initial condition, for example, $\lambda = 1.1$, lead to blow-up solutions. For example,

$$u_0(r, \theta) = 1.1 Q(r \cos \theta + 4.5, r \sin \theta)$$

blows up at time $t = 0.84$ with the diverging L^∞ norm as shown in Figure 5. We use the Newton iteration to solve the implicit scheme (2.3) and to reach the desired accuracy. It is quite challenging to approach the blow-up time while maintaining the convergence of the Newton iteration (2.5). To address this issue, we run the scheme with a more refined mesh in order to maintain the convergence of (2.5). This is not a simple task to perform in the $2d$ non-radial case and can become computationally prohibitive. However for our results of identifying the blow-up and the type of interaction, it suffices to investigate the L^∞ -norm (or the height) and label the solution as ‘the blow-up’ if, for example, the amplitude becomes 3 times higher than the initial one (e.g., see the right graph in Figure 5).

The solution u at $t=0.84$

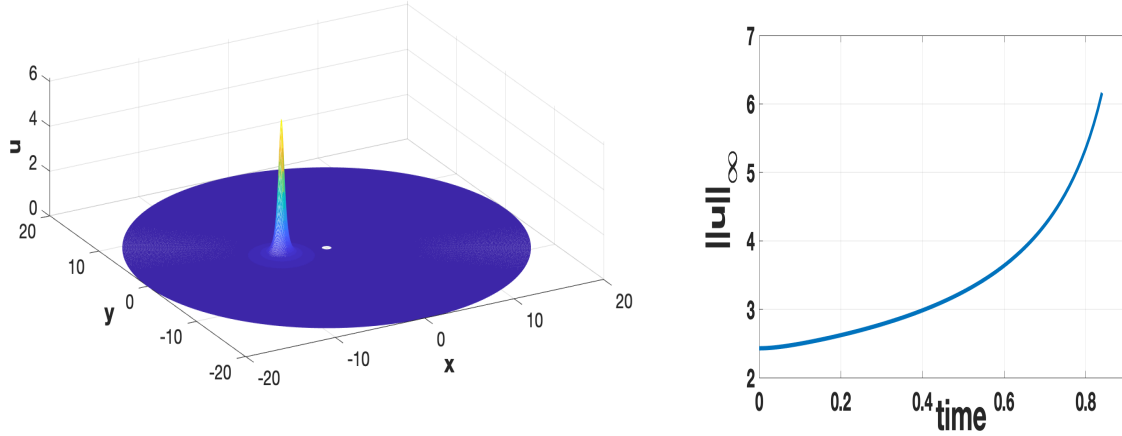


FIGURE 5. Ground state solution to the 2d cubic NLS_Ω equation with $u_0(x, y) = 1.1 Q(x + 4.5, y)$ at $t = 0.84$ (left) and its L^∞ norm depending on time (right).

We next examine the initial condition of the perturbed soliton with the mass smaller than that of the ground state (i.e., $\|u_0\|_{L^2} < \|Q\|_{L^2}$), for example,

$$u_0(r, \theta) = 0.9 Q(r \cos \theta + 4.5, r \sin \theta).$$

The solution u at $t=1.5$

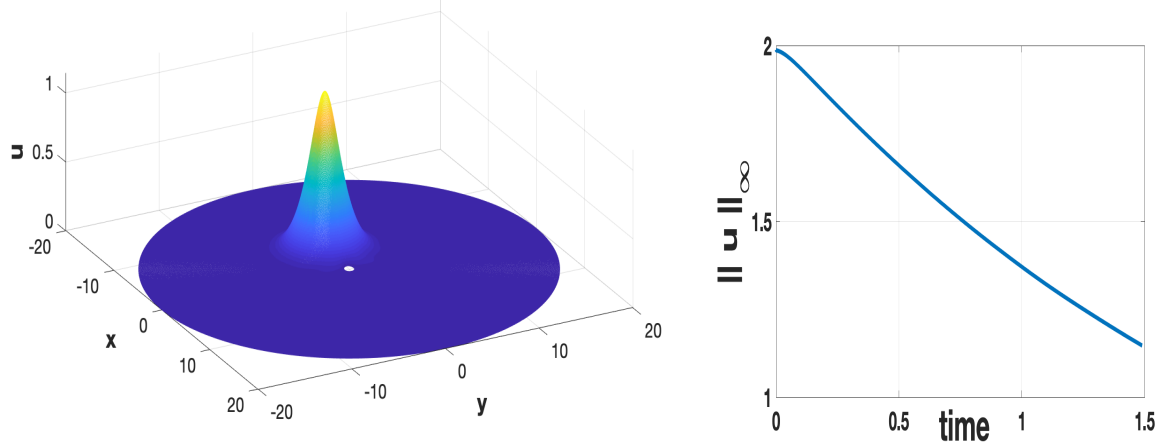


FIGURE 6. Ground state solution to the 2d cubic NLS_Ω with $u(x, y, 0) = 0.9 Q(x + 4.5, y)$ at $t = 1.5$ (left) and the L^∞ norm for $0 < t < 1.5$ (right).

A snapshot of the corresponding solution to the NLS_Ω equation at time $t = 1.5$ and the time dependence of the L^∞ norm are shown in Figure 6. In this example, one can see that the L^∞ norm is monotonously decreasing with a definite negative slope. It is plausible to conclude that this solution disperses in a long run, as expected in the L^2 -critical case for the perturbations with smaller mass than that of the soliton (note that $\lambda = 0.9 < 1$). To further confirm our expectations we run this example with the same initial condition for longer times and the next Figure 7 shows that the L^∞ norm indeed keeps decreasing to 0.

We have tried other perturbations of Q with various shifts and observed similar behavior. Therefore, we confirm in this section that the threshold for blow-up vs. scattering for the perturbed soliton data is indeed given by the ground state.

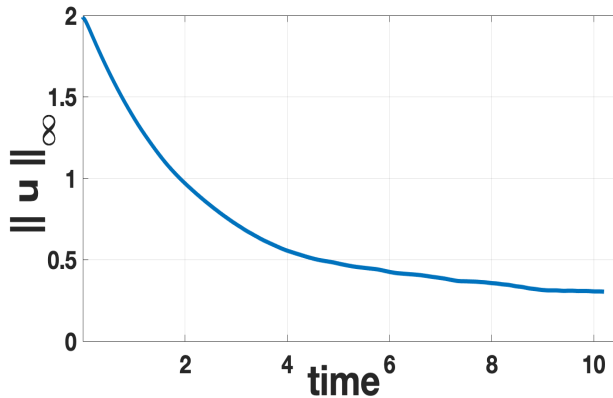


FIGURE 7. Time dependence of the L^∞ -norm for the solution in Figure 6.

Remark. In the rest of the paper, except Section 9, we consider a shifted Gaussian initial data u_0 as in (2.2). One of the reasons is that it has a faster decay than the ground state (though both decay exponentially), which ensures that the simulations close to the obstacle satisfy Dirichlet boundary condition (even a slightly faster exponential decay makes computations easier). Another reason is that in order to study various interactions with an obstacle, we consider initial data u_0 with the minimal possible distance d^* to the obstacle (as defined in (1.10)) so that u_0 is smooth and still satisfies Dirichlet boundary condition.

5. DEPENDENCE ON THE DISTANCE

From now on we study both the $2d$ cubic and quintic NLS $_\Omega$ equations ($p = 3, 5$) with the radius of the obstacle $r_\star = 0.5$. Our goal in this section is to consider solutions with data u_0 such that the distance d between the obstacle and the initial condition is larger than the minimal distance d^* .

We take (2.2) with x_c and y_c such that $d \gg d^*$. As before $v = (v_x, v_y)$ is the velocity vector, which governs the moving direction of the initial bump. Figure 8 shows different directions of propagation for this solitary wave-type data depending on the velocity \vec{v} .

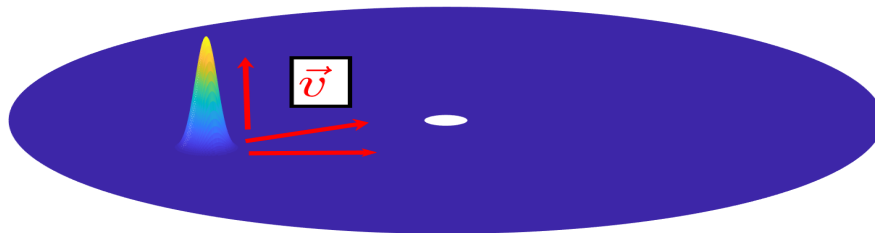


FIGURE 8. Directions of the velocity \vec{v} of the initial data (single bump) relative to an obstacle (the white region represents the location of the obstacle). If the initial bump is relatively far from the obstacle, $d \gg d^*$, then the blow-up occurs in any direction of the initial velocity shown on the picture, for example, as it is shown in Figure 9.

5.1. **The L^2 -critical case.** For the $2d$ cubic NLS $_{\Omega}$ equation we take the initial data (2.2) with large enough mass and $d \gg d^*$. Then the corresponding solution to (2.3) blows up in finite time before reaching or interacting with an obstacle in any direction of the velocity vector v , see Figure 9.

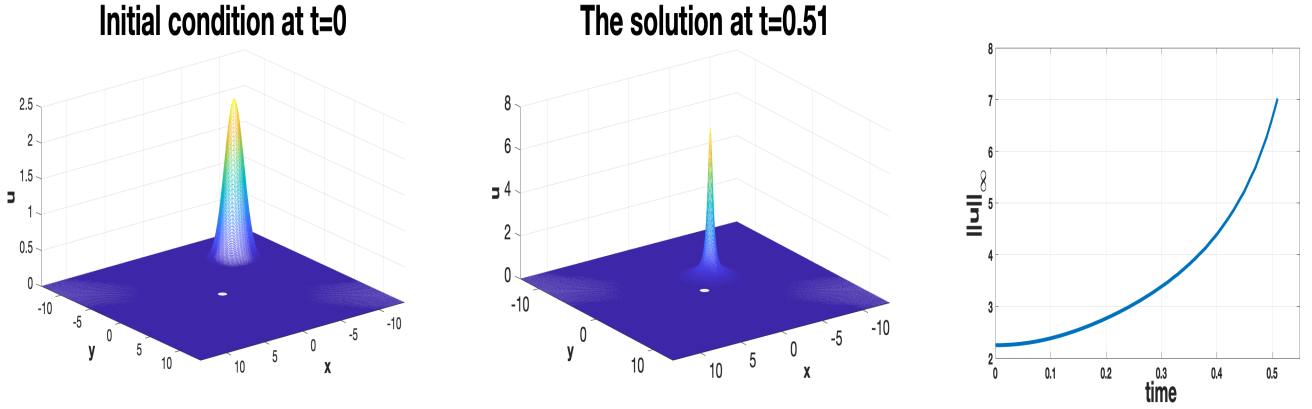


FIGURE 9. Snapshots of the initial data u_0 as in (2.2) with large enough mass and the solution $u(t)$ to the $2d$ cubic NLS $_{\Omega}$ at $t = 0$ and $t = 0.51$ with $d \gg d^*$ (left and middle); the L^{∞} -norm depending on time (right).

Later we study the case when $d \equiv d^*$ and the solution concentrates in its (blow-up) core after the obstacle, for the same initial data but with a different velocity direction. We also investigate the influence of the obstacle when there is an interaction between the traveling wave and the obstacle. In Section 6.1, we consider the weak interaction for the $2d$ cubic NLS $_{\Omega}$ equation (L^2 -critical case) and in Section 7.1 we study the strong interaction. We observe that in those cases the solution exhibits a different behavior on a longer time interval.

5.2. **The L^2 -supercritical case.** Next, we consider the $2d$ quintic NLS $_{\Omega}$ equation and take the initial condition (2.2) with a large mass and $d \gg d^*$. In the following scenario, we fix parameters A_0 and $v = (v_x, 0)$ and vary the translation parameter y_c in the translation (x_c, y_c) as shown in Figure 10.

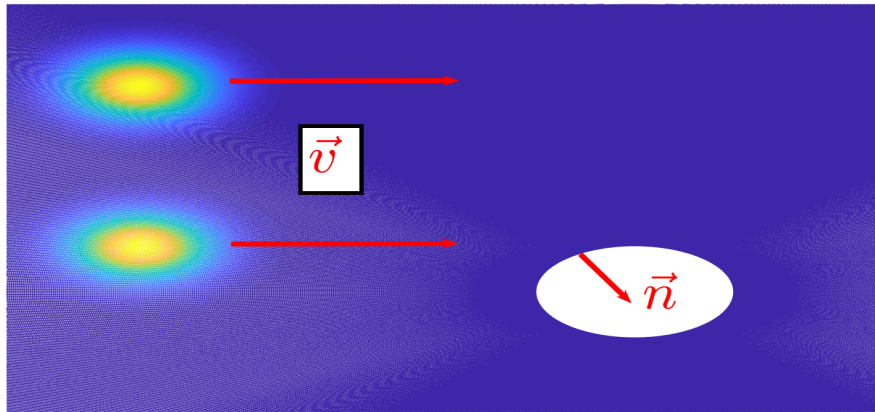


FIGURE 10. Directions of the velocity \vec{v} of the initial two single bumps that move along either the line $y = 5$ or $y = 2$ with $d \gg d^*$.

Snapshots of the corresponding solution to the $2d$ quintic NLS $_{\Omega}$ equation are plotted in Figure 11. As in the previous example, the solution blows up in finite time before the obstacle (for large x_c).

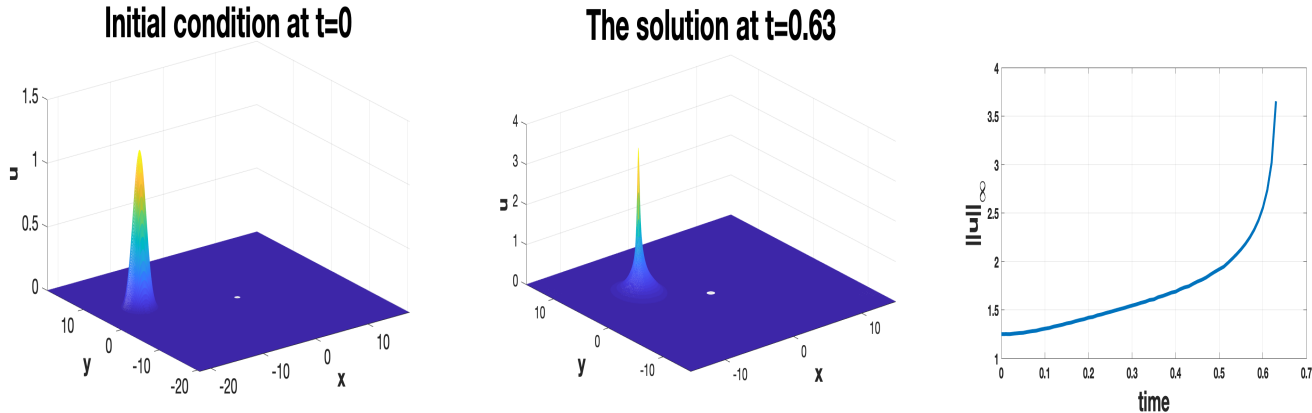


FIGURE 11. A blow-up solution to the $2d$ quintic NLS $_{\Omega}$ equation with the initial condition (2.3) and $d \gg d^*$. The initial profile (left), a snapshot of the solution at $t = 0.63$ (middle), the time dependence of the L^{∞} -norm (right).

We later investigate the case when the solution blows up in finite time, after the obstacle and when $d \equiv d^*$, with the same initial data u_0 as in (2.2) for a fixed amplitude $A_0 = 1.25$ and velocity direction $v = (15, 0)$, and $x_c = -4.5$, but for different space translation y_c , see Table 2. This will lead to the weak or strong interaction for the $2d$ quintic NLS $_{\Omega}$ equation (L^2 -supercritical case), see Sections 6.2 and 7.2.

6. WEAK INTERACTION WITH AN OBSTACLE

6.1. The L^2 -critical case. We return to the cubic NLS $_{\Omega}$ setting and consider initial data (2.2) with $A_0 = 2.25$, $x_c = -4.5$, $y_c = -4.5$ and we vary the direction of the velocity vector. Considering the two scenarios, as shown in Figure 12.

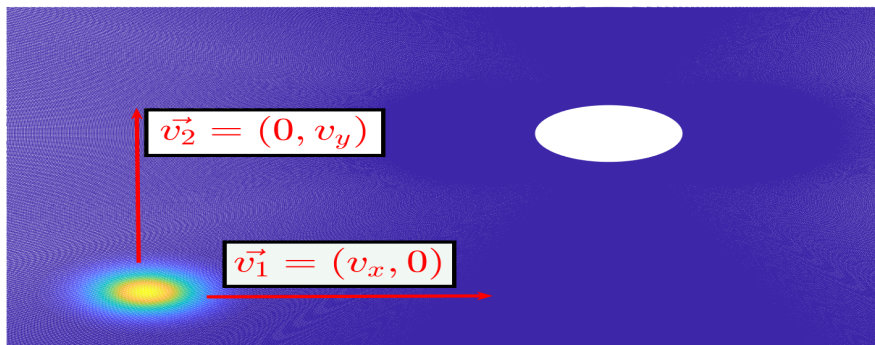


FIGURE 12. Directions of the velocity for the examples in Section 6.1.

We start with $v_1 = (v_x, 0)$, $v_x = 15$, and observe that the solution blows up at time $t = 0.52$. It does not interact with the obstacle; its behavior is the same as it would be of a solitary wave on the whole space, see Figure 13.

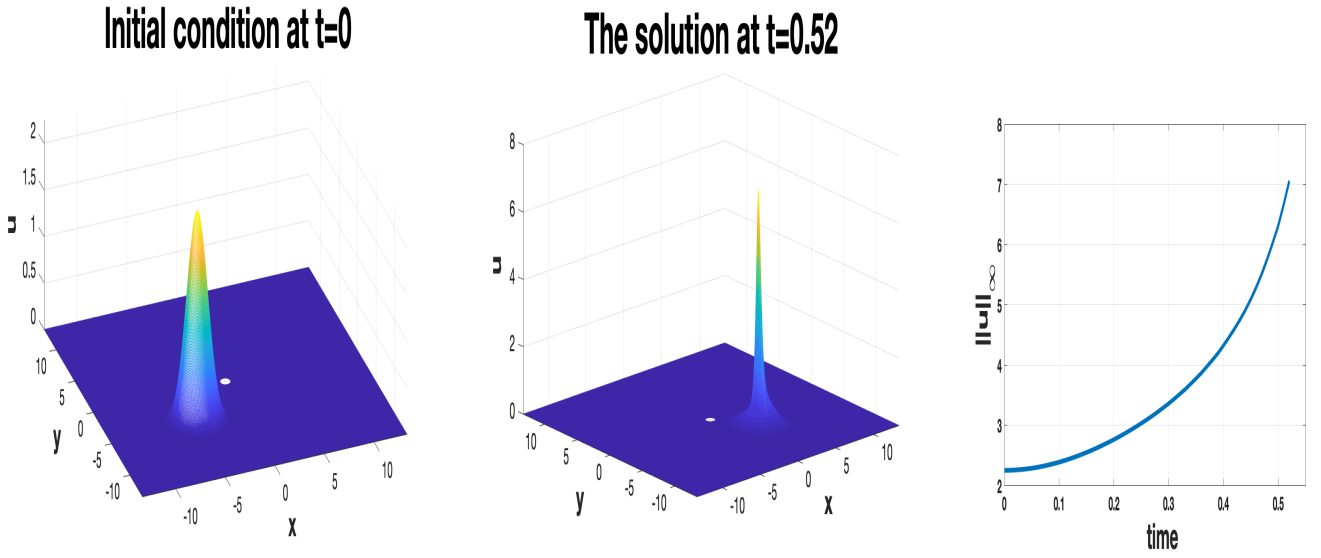


FIGURE 13. The 2d cubic NLS_{Ω} with u_0 from (2.2), $A_0 = 2.25$, $x_c = -4.5$, $y_c = -4.5$ and $v_1 = (15, 0)$ (left); the time evolution at $t = 0.52$ (middle); the time dependence of the L^{∞} -norm (right).

Next, we take the same initial condition but with the velocity vector $v_2 = (0, v_y) = (0, 15)$, that is, perpendicular to the direction used in the previous example, as shown in Figure 12. We observe, see Figure 14, that the solution blows up at the same time.

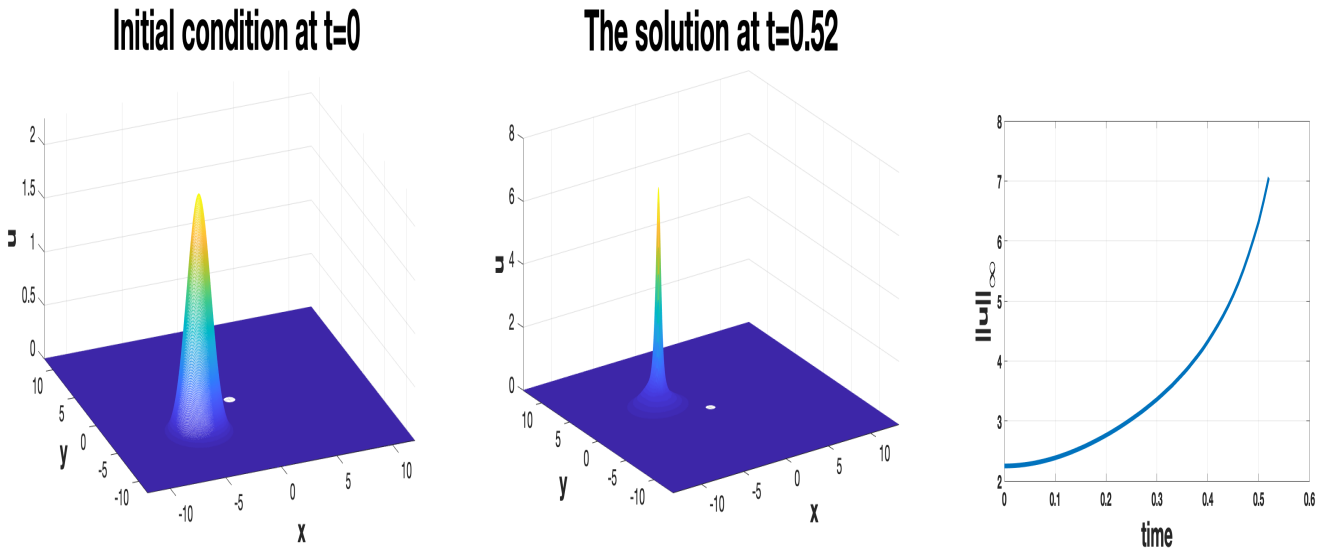


FIGURE 14. The 2d cubic NLS_{Ω} equation with u_0 from (2.2), $A_0 = 2.25$, $x_c = -4.5$, $y_c = -4.5$ and $v_2 = (0, 15)$ (left); its time evolution at $t = 0.52$ (middle); the time dependence of the L^{∞} -norm (right).

In our third example, we take the initial condition u_0 from (2.2) with $A_0 = 2.25$, $x_c = -4.5$, $y_c = -4.5$ and the velocity \vec{v} that has a different direction but has the same magnitude $|\vec{v}|$, as in the previous two examples: we choose $v_1 = (v_x, v_y)$ and $v_2 = (v_y, v_x)$ as shown on Figure 15.

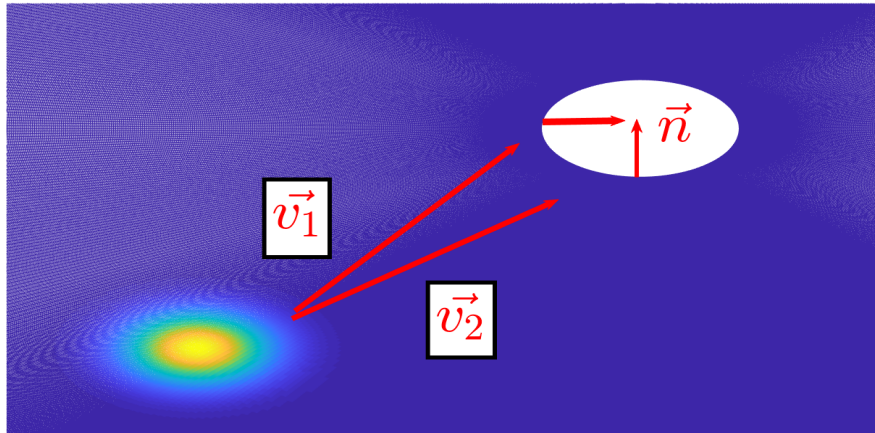


FIGURE 15. The directions of the velocity for the examples in Figures 16 to 19.

We choose $v_1 = (15, 9)$ such that the solution has a small interaction with the obstacle. After the collision, we observe that the solution has almost the same behavior (as in Figures 13, 14), i.e., it blows up but with slightly dispersive reflection part, preserving the shape of the soliton, similar to the two previous cases. The solution blows up in finite time $t = 0.57$ after the interaction with the obstacle, see Figure 16. Moreover, we see that at the collision time the L^∞ -norm has a slight perturbation (or a small oscillation), however, afterwards it continues to increase: such perturbation is not sufficient to prevent the overall growing of the L^∞ -norm and the occurrence of the blow-up, however, it affects the blow-up time compared to the previous examples. Besides Figure 16 with the L^∞ norm dependence, we also provide snapshots of the behavior of the solution for different time steps for $v_2 = (9, 15)$ in Figure 17.

The solution at t=0.57

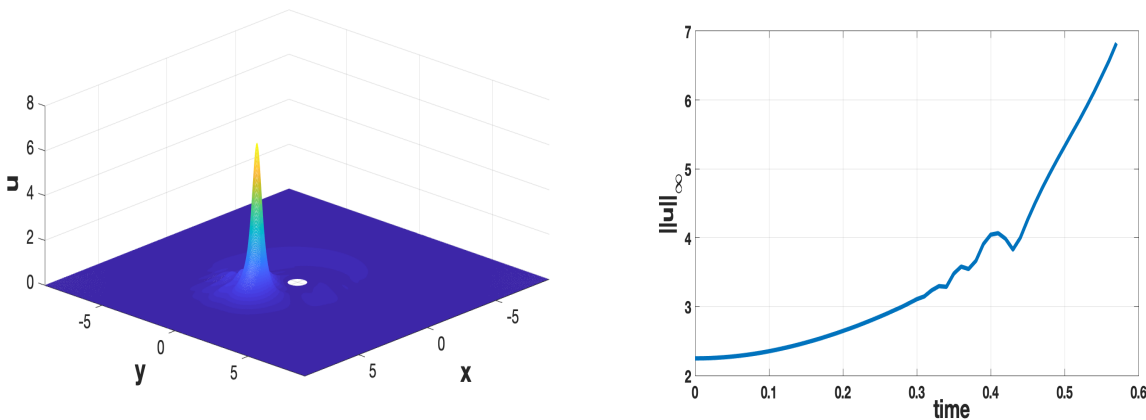


FIGURE 16. Solution to the $2d$ cubic NLS_Ω equation with the initial condition u_0 as in (2.2), $A_0 = 2.25$, $x_c = -4.5$, $y_c = -4.5$, and $v_1 = (15, 9)$ at time $t = 0.57$, moving on the line $y = \frac{3}{5}x$ (left); the time dependence of L^∞ -norm (right).

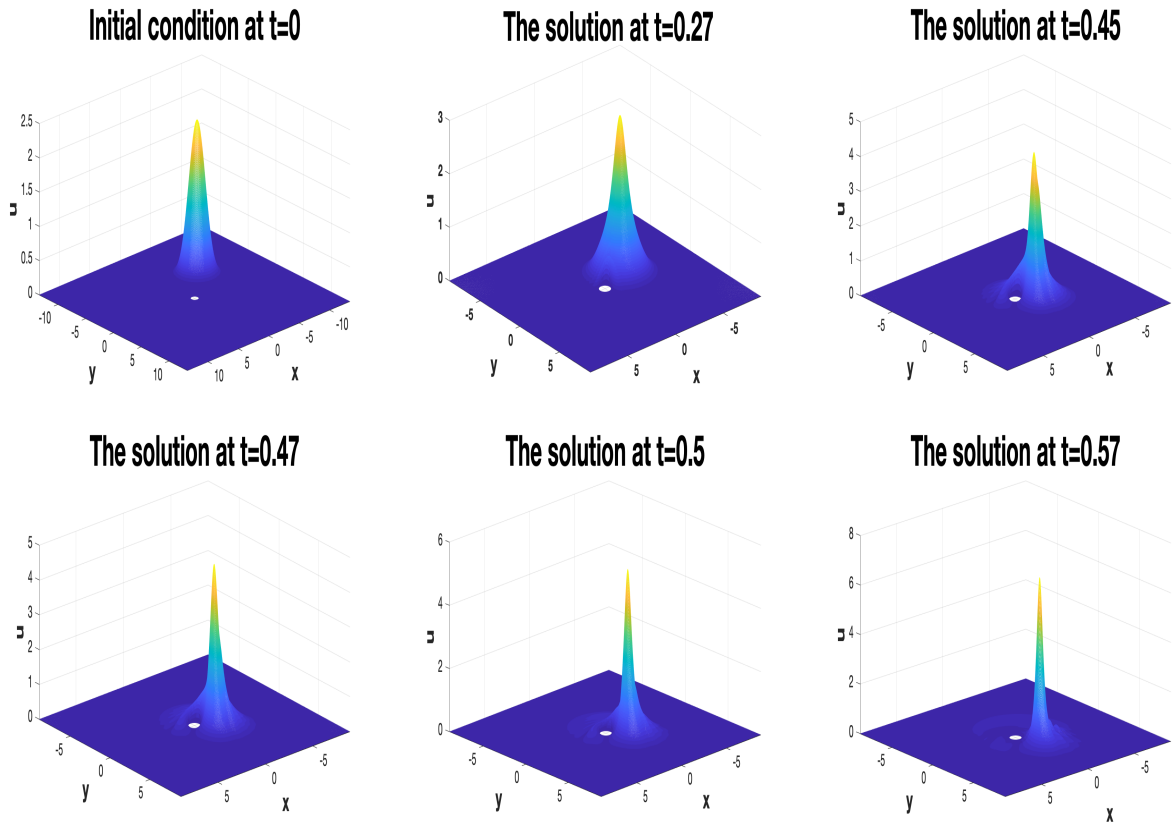


FIGURE 17. Snapshots of the solution $u(t)$ to the $2d$ cubic NLS_Ω equation with the initial condition u_0 as in (2.2), $A_0 = 2.25$, $x_c = -4.5$, $y_c = -4.5$ and $v_2 = (9, 15)$, moving on the line $y = \frac{5}{3}x$.

In our fourth example here, we consider the initial condition u_0 from (2.2) with $A_0 = 2.25$, $x_c = -4.5$, $y_c = -4.5$ and the velocity vector $v_1 = (12, 15)$ and $v_2 = (15, 12)$. For $v_1 = (12, 15)$, a snapshot of the solution at time $t = 1.2$ is plotted on the left of Figure 18. The right subplot shows the L^∞ -norm depending

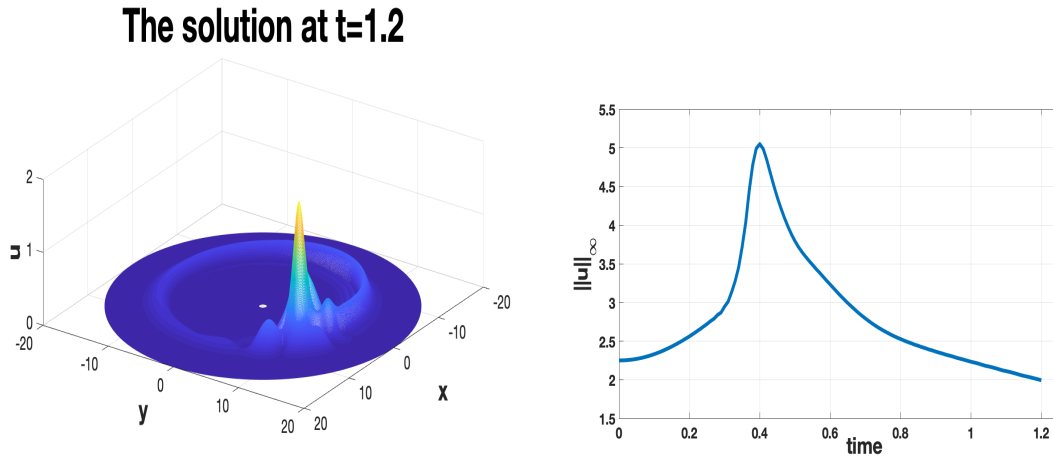


FIGURE 18. Solution to the $2d$ cubic NLS_Ω equation with the initial condition u_0 from (2.2), $A_0 = 2.25$, $(x_c, y_c) = (-4.5, -4.5)$ and $v_1 = (12, 15)$ at time $t = 1.2$ moving on the line $y = \frac{5}{4}x$ (left), the time dependence of the L^∞ -norm of the solution (right).

on time, which appears to grow quite fast in the beginning of the simulation, but after the collision it starts to decrease monotonically. This solution disperses, or in other words, it becomes a scattering solution. Thus, the obstacle arrests the blow-up. This is a **different behavior** compared to the previous examples, where the solutions were transmitted almost with the same shape after the interaction and the soliton core was preserved. Unlike the previous examples, the collision of the solution with the obstacle here creates reflected waves, which then disperse the solution. The reflection causes the loss of the mass in the main part of the solution, arresting the blow-up in finite time unlike the examples above, where the reflection does not affect the blow-up of the solution and only delays the blow-up time. In this case the interaction between the soliton and the obstacle has a substantial influence on the behavior of the solution, which is a completely new dynamics compared to the dynamics on the whole space. For better understanding of this dynamics, we provide snapshots of the behavior of the solution for different time steps for $v_2 = (15, 12)$, see Figure 19. This is an example where the solution has a behavior close to the *strong* interaction case.

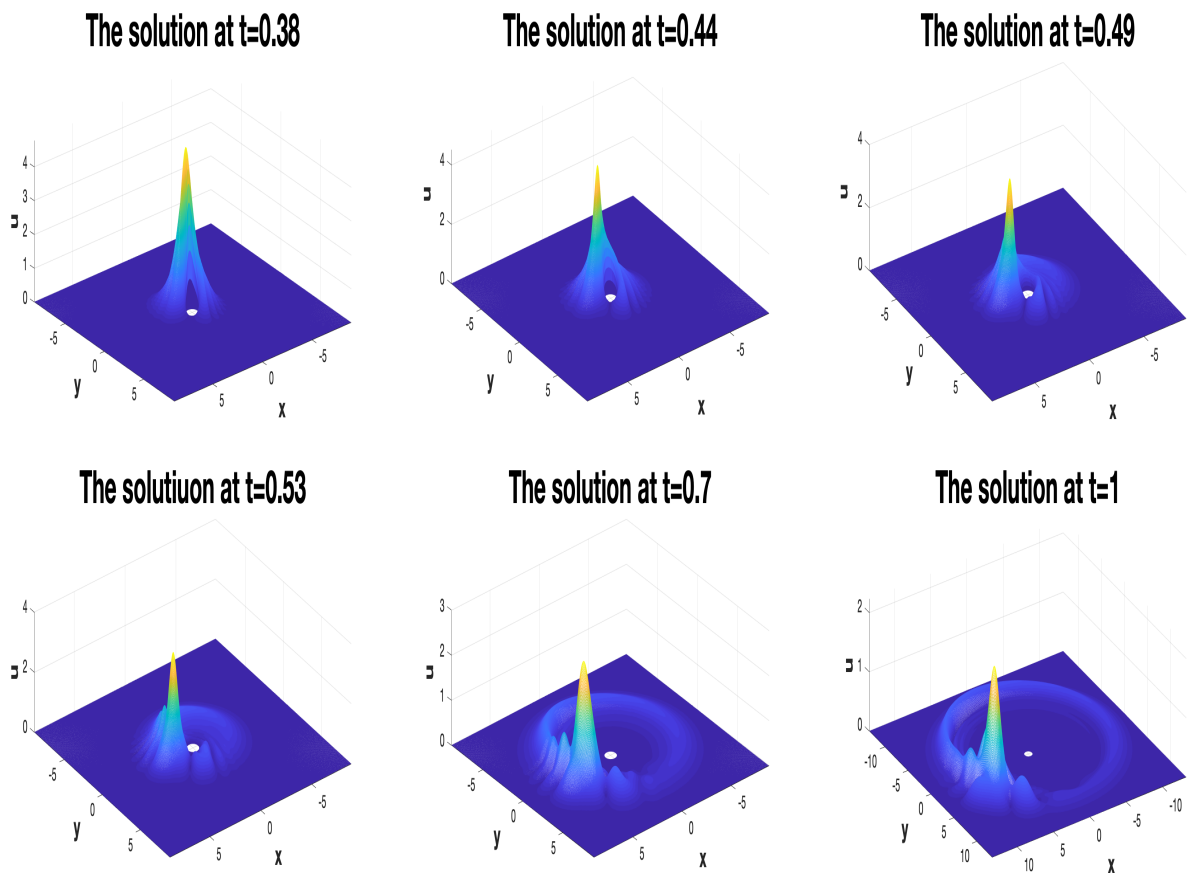


FIGURE 19. Snapshots of the solution $u(t)$ to the $2d$ cubic NLS_{Ω} equation, with the initial condition u_0 from (2.2), $A_0 = 2.25$, $(x_c, y_c) = (-4.5, -4.5)$ and $v_2 = (15, 12)$ moving on the line $y = \frac{4}{5}x$.

In the following simulations, we study the behavior of various examples of solutions to the cubic NLS_{Ω} equation, depending on the interaction between the solution and the obstacle. We consider the same initial condition as in (2.2), we fix the following parameters as follows: $A_0 = 2.25$, $x_c = -4.5$, $y_c = -4.5$, and vary the direction of the velocity vector (v_x, v_y) .

We record the results of our simulations for this L^2 -critical case in Table 1.

(v_x, v_y)	Discrete mass	Discrete energy	Behavior of the solution	Type of interaction
(15, 0)	15.9043	442.9353	Blow-up at $t \approx 0.52$	no-interaction
(0, 15)	15.9043	442.9353	Blow-up at $t \approx 0.52$	no-interaction
(15, 8)	15.9043	570.4814	Blow-up at $t \approx 0.56$	weak-interaction
(8, 15)	15.9043	570.4814	Blow-up at $t \approx 0.56$	weak-interaction
(9, 15)	15.9043	604.0182	Blow-up up $t \approx 0.57$	weak-interaction
(15, 9)	15.9043	604.0182	Blow-up at $t \approx 0.57$	weak-interaction
(10, 15)	15.9043	641.4737	Blow-up at $t \approx 0.63$	weak-interaction
(15, 10)	15.9043	641.4737	Blow-up at $t \approx 0.63$	weak-interaction
(15, 12)	15.9043	728.1404	Scattering	weak-interaction
(12, 15)	15.9043	728.1404	Scattering	weak-interaction
(15, 15)	15.9043	887.5015	Scattering	strong-interaction

TABLE 1. Different velocity directions $\vec{v} = (v_x, v_y)$ and the corresponding behavior of the solution $u(t)$ to the 2d cubic (NLS $_{\Omega}$) with the indicated discrete mass and energy (the value of energy differs due to the phase).

6.2. The L^2 -supercritical case. We now consider the 2d quintic NLS $_{\Omega}$ equation ($p = 5$). Again, we try to carefully examine the interaction between the obstacle and the solution. In the following simulations, we fix A_0 and the velocity v , but vary the translation parameters. We start with an example, where there is no interaction in order to compare the behavior of the solution for different scenarios later, especially when there will be a strong interaction. For that, we consider the initial data u_0 from (2.2) with

$$A_0 = 1.25, \quad x_c = -4.5, \quad y_c = 5, \quad \text{and} \quad v = (15, 0), \quad (6.1)$$

which can be seen on the left of Figure 20. The middle subplot shows that the corresponding solution to

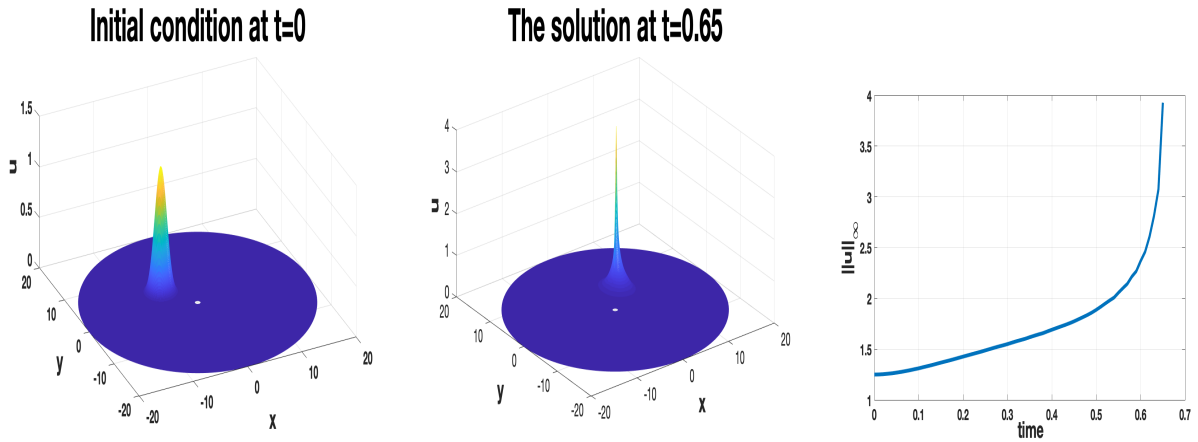


FIGURE 20. Solution to the 2d quintic NLS $_{\Omega}$ equation with u_0 from (2.2) and (6.1) (left) close to blow-up time (middle); time dependence of the L^∞ -norm (right).

the 2d quintic NLS $_{\Omega}$ equation blows up in finite time at $t = 0.65$ with the diverging L^∞ -norm. Snapshots of the solution in time (top view onto the xy -plane) are plotted in Figure 21. We observe that the solution blows up in finite time and there is no interaction between the solution and the obstacle.

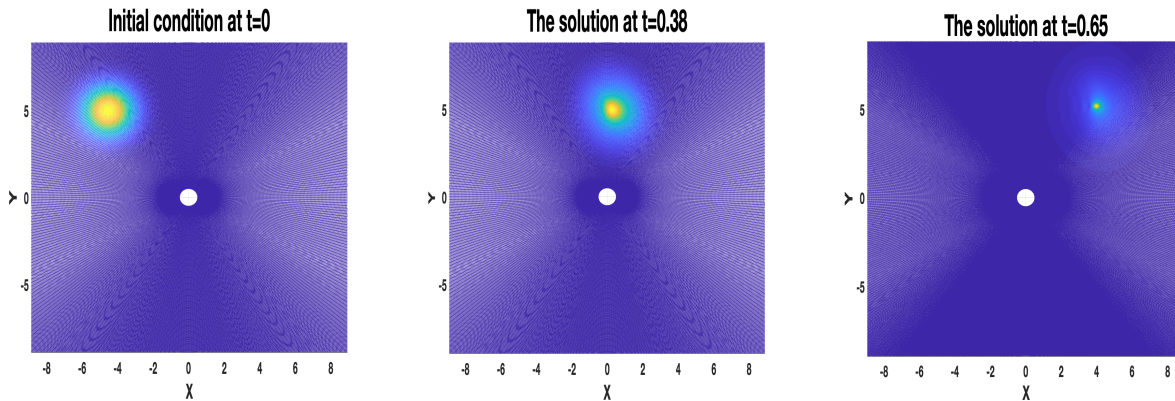


FIGURE 21. Snapshots of the evolution of u_0 from (2.2) with (6.1) at $t = 0$, $t = 0.38$ and $t = 0.65$.

Next, we take the same initial data u_0 as in the previous example (i.e., $A_0 = 1.25$, $v = (15, 0)$, $x_c = -4.5$) except for the y_c value we choose $y_c = 2$ as shown in Figure 10. In this case, we expect that the traveling wave solution has some weak interaction with the obstacle, see Figure 22.

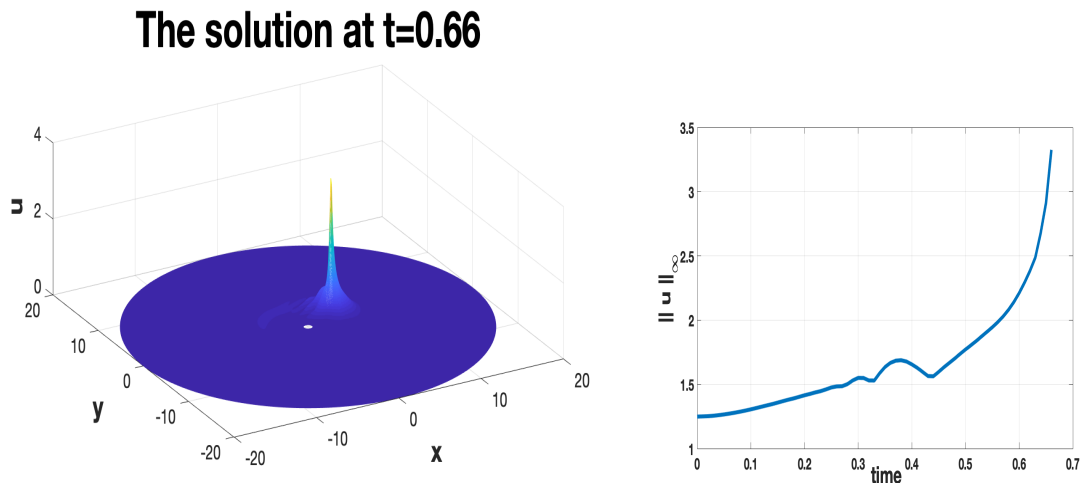


FIGURE 22. Solution $u(t)$ to the $2d$ quintic NLS_Ω equation with initial condition u_0 from (2.2), where $A_0 = 1.25$, $v = (15, 0)$ and $(x_c, y_c) = (-4.5, 2)$. A snapshot of $u(t)$ at $t = 0.66$ (left), the time dependence of the L^∞ -norm (right).

We observe that with this weak interaction, the solution still blows up in finite time at $t = 0.66$, but the blow-up time is delayed compared to the case, where there was no interaction between the solution and the obstacle, compare Figures 11 and 22. Moreover, we observe a slight perturbation of the growth in the L^∞ -norm: at the collision, the amplitude of the solution starts decreasing but after the weak interaction, the solution is back to the concentration leading to the blow-up. This can be explained by the appearance of small reflected waves after the collision, which scatter at the end of the simulation. They can be seen in the snapshots of the solution in Figure 23 with the view onto the xy -plane and zooming near the obstacle.

Next, we summarize the behavior of the solution to the $2d$ quintic NLS_Ω equation, depending on the initial parameters. We take different values for the space translation y_c in the initial condition (2.2) and fix the following parameters:

$$A_0 = 1.25, \quad v_x = 15, \quad v_y = 0, \quad x_c = -4.5.$$

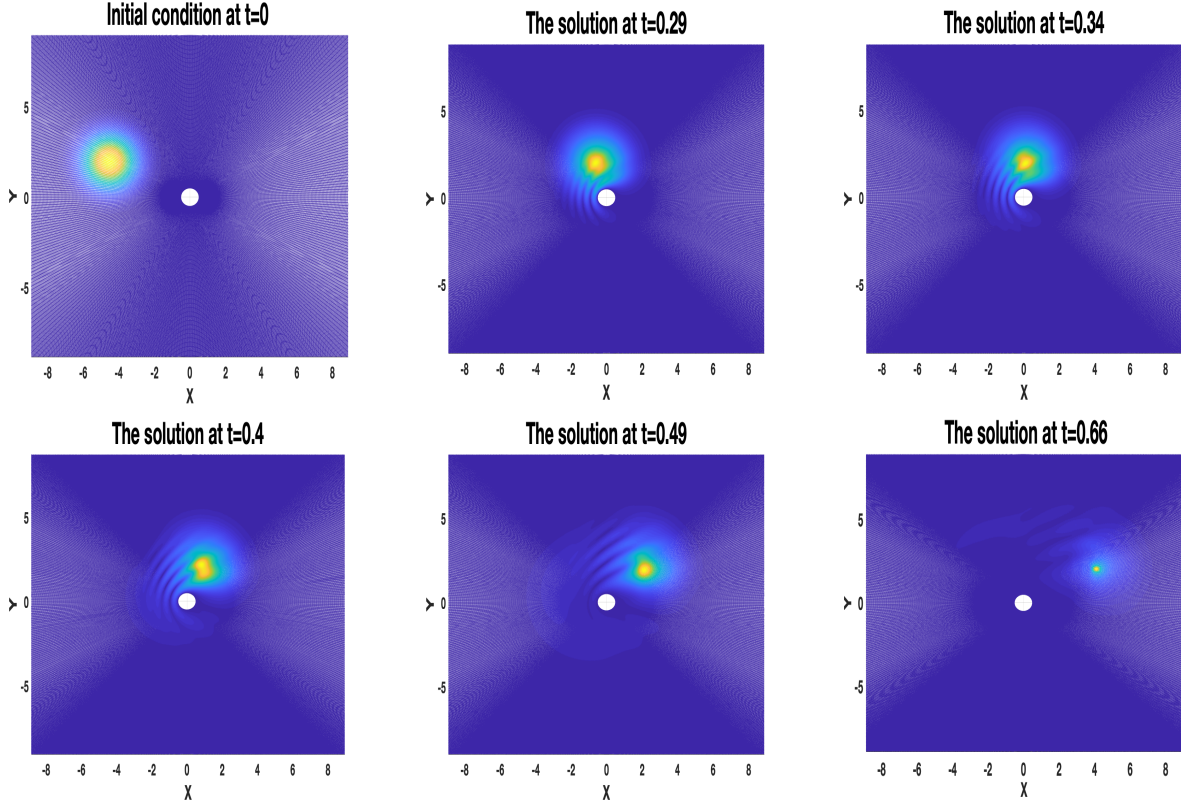


FIGURE 23. Snapshots of the time evolution of $u(t)$ with initial condition u_0 from (2.2), $A_0 = 1.25$, $v = (15, 0)$ and $(x_c, y_c) = (-4.5, 2)$, which eventually blows up in finite time.

The results are given in Table 2.

(x_c, y_c)	Discrete mass	Discrete energy	Behavior of the solution	Type of interaction
$(-4.5, 5)$	4.9087	138.9766	Blow-up at $t \approx 0.65$	no interaction
$(-4.5, 4)$	4.9087	139.2859	Blow-up at $t \approx 0.68$	no interaction
$(-4.5, 3)$	4.9087	139.4553	Blow-up at $t \approx 0.65$	weak-interaction
$(-4.5, 2)$	4.9087	139.5022	Blow-up at $t \approx 0.66$	weak-interaction
$(-4.5, 1.5)$	4.9087	139.4946	Blow-up at $t \approx 0.51$	weak-interaction
$(-4.5, 1)$	4.9087	139.4784	Blow-up at $t \approx 0.41$	weak-interaction
$(-4.5, 0.5)$	4.9087	139.4636	Scattering	weak-interaction
$(-4.5, 0)$	4.9087	139.4578	Scattering	strong-interaction
$(-4.5, -0.5)$	4.9087	139.4636	Scattering	weak-interaction
$(-4.5, -1)$	4.9087	139.4784	Blow-up at $t \approx 0.4$	weak-interaction
$(-4.5, -1.5)$	4.9087	139.4946	Blow-up at $t \approx 0.5$	weak-interaction
$(-4.5, -2)$	4.9087	139.0924	Blow-up at $t \approx 0.63$	weak-interaction

TABLE 2. Influence of the translation parameter y_c on the behavior of the solution $u(t)$ with initial data (2.2), $A_0 = 1.25$, $v = (15, 0)$. Note that a tiny difference in the values of the discrete energy for different y_c results from the varying density of the mesh grid: this is due to the fact that the polar coordinates (r, θ) form a uniform mesh, however, $(x, y) = (r \cos \theta, r \sin \theta)$ will not be uniform. Nevertheless, the discrete energy is conserved in each case from the start, i.e., $E[u^n] = E[u^0]$ in each simulation.

7. STRONG INTERACTION WITH AN OBSTACLE

7.1. **The L^2 -critical case.** We now consider a direct interaction of the solution with an obstacle, which we term as a *strong* interaction, starting with the L^2 -critical case. The depiction of the velocity direction and the initial location is in Figure 24.

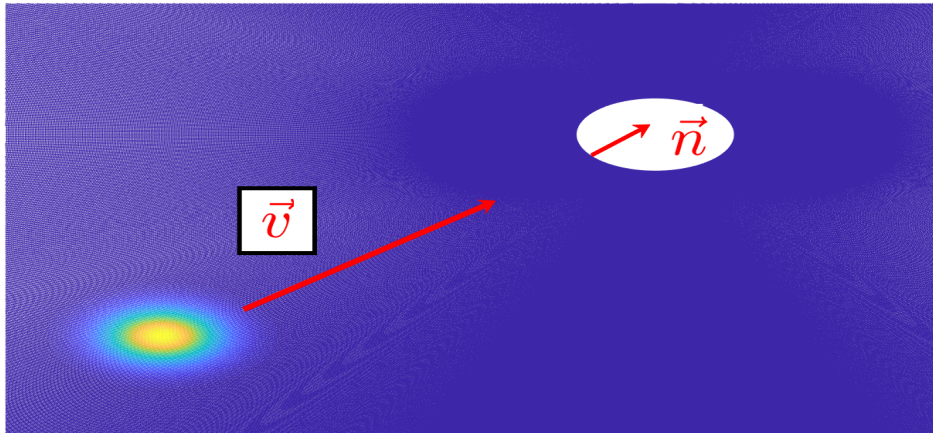


FIGURE 24. The directions of the velocity of the solution $u(t)$ on the line $y = x$ and the same direction of the outward normal vector \vec{n} .

We consider the cubic NLS_Ω equation with the same initial data (2.2), with the same amplitude and space translation ($A_0 = 2.25$, $(x_c, y_c) = (-4.5, -4.5)$), as in Subsection 6.1 but in this case we take the velocity directly pointed at the obstacle $v = (15, 15)$, meaning that the solution $u(t)$ is moving along the line $y = x$, i.e., in the same direction as the outward normal vector \vec{n} as shown in Figure 24.

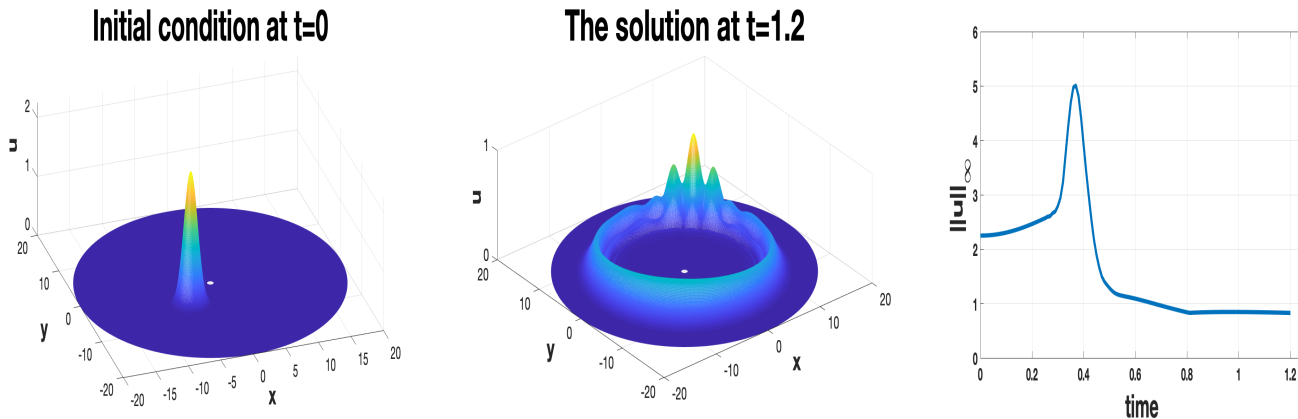


FIGURE 25. The initial condition u_0 at $t = 0$ from (2.2), $A_0 = 2.25$, $(x_c, y_c) = (-4.5, -4.5)$ and $v = (15, 15)$ (left); the corresponding solution $u(t)$ to the 2d cubic NLS_Ω equation at $t = 1.2$ (middle); time dependence of L^∞ norm (right).

In this scenario, we observe that the solution has a scattering behavior and does not conserve the same profile or shape of the initial form of the solitary wave, see Figure 25, thus, exhibits the strong interaction. Snapshots of the time evolution of this solution $u(t)$ to show the strong interaction are given in Figure 26:

the solution hugs the obstacle while transferring the mass forward, then it forms the two main bumps in front of the obstacle, later they connect together, which creates a third (middle) bump and shifts more and more mass into this central lump while propagating it forward along the main velocity line ($y = x$ in this case). The circle of dispersive reflective waves (including backward reflective waves) forms and expands, radiating out all of the reflective waves.

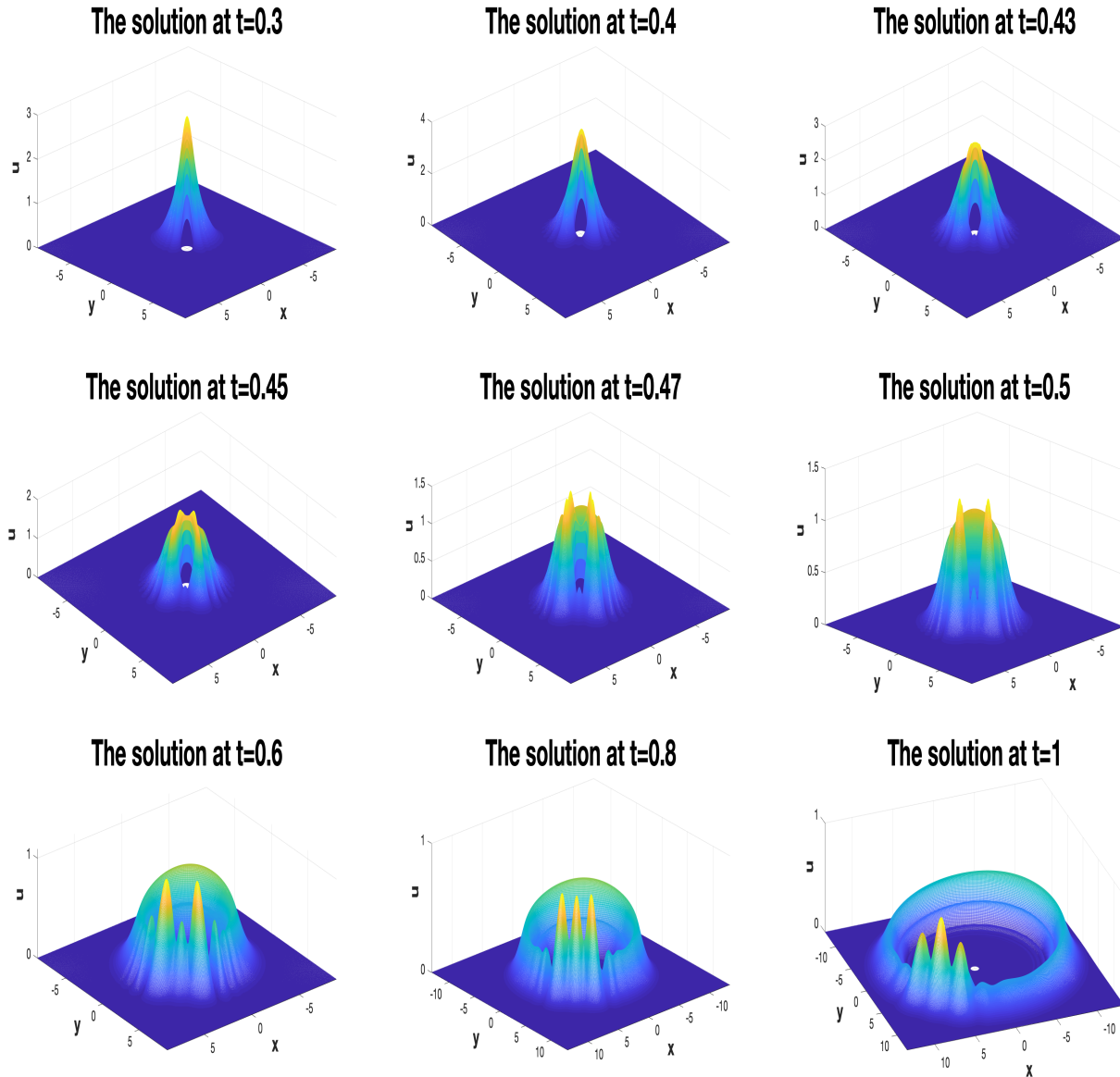


FIGURE 26. Snapshots of the solution $u(t)$ to the $2d$ cubic NLS_{Ω} equation for different time steps of the strong-interaction between the solution and the obstacle with the initial data as in Figure 25.

The obstacle transforms the blow-up behavior into what seems to be scattering, that we investigate further. Before doing that, we emphasize that the strong interaction has a substantial influence on the dynamics of the solution. We point out that in the weak interaction case in a similar example in Section 6.1 (L^2 -critical case) the solution blows up in finite time. In the considered case, the L^{∞} -norm starts increasing, manifesting a blow-up behavior, see Figure 25, however, after the collision, the amplitude of the solution

start decreasing. After that, we observe that the L^∞ -norm appears to stabilize, as shown in the right graph in Figure 25, where $\|u(t)\|_\infty \approx 0.8$ after the interaction, indicating that the solution might not be scattering (for example, it could approach a rescaled soliton). We check this case simulating it for a longer time and observe that the L^∞ -norm continues to decrease as shown in the left subplot of Figure 27. In the right graph we show the solution amplitude change in time on a log scale for $t \in [2, 3.32]$, which shows that it is decreasing as $\frac{1}{\sqrt{t}}$. Thus, it is plausible to conclude that the solution scatters (however, this would have to be proved analytically, as it is possible that it might approach an asymptote at a later time).

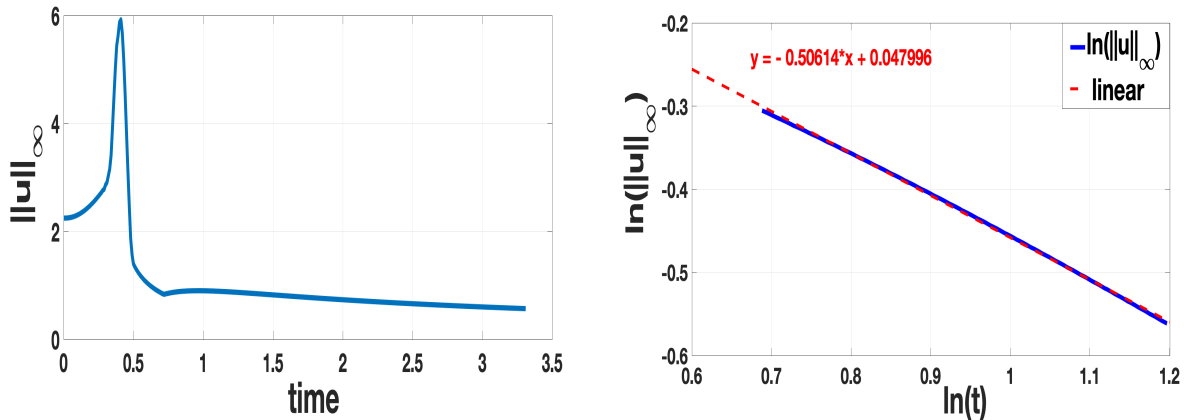


FIGURE 27. The time dependence of L^∞ norm (left); the slope of the L^∞ norm from $t = 2$ to $t = 3.32$ on a log scale (right).

7.2. The L^2 -supercritical case. In the $2d$ quintic NLS $_\Omega$ equation ($p = 5$), we also investigate the *strong* interaction between the obstacle and the solution, where the solution is moving in the same direction as the outward normal vector of the obstacle, see Figure 28.

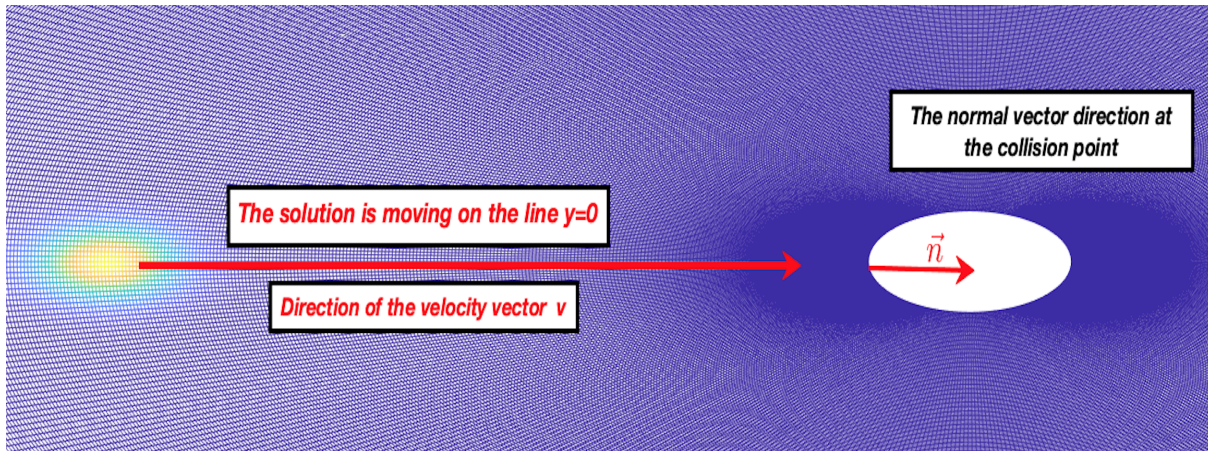


FIGURE 28. The direction of movement of the solution, on the line $y = 0$ with outward normal vector.

We consider the same initial data (2.2), with the same phase as for the quintic NLS $_\Omega$ equation described in Section 6.2 but now with $y_c = 0$ (i.e., $A_0 = 1.25$, $x_c = -4.5$ and $v = (v_x, 0)$ are fixed parameters). In the present situation, the solution is moving on the line $y = 0$, i.e., in the same direction as the outward normal vector of the obstacle. The solitary wave hits the obstacle straight on, causing a strong interaction between the wave and the obstacle, see Figure 29.

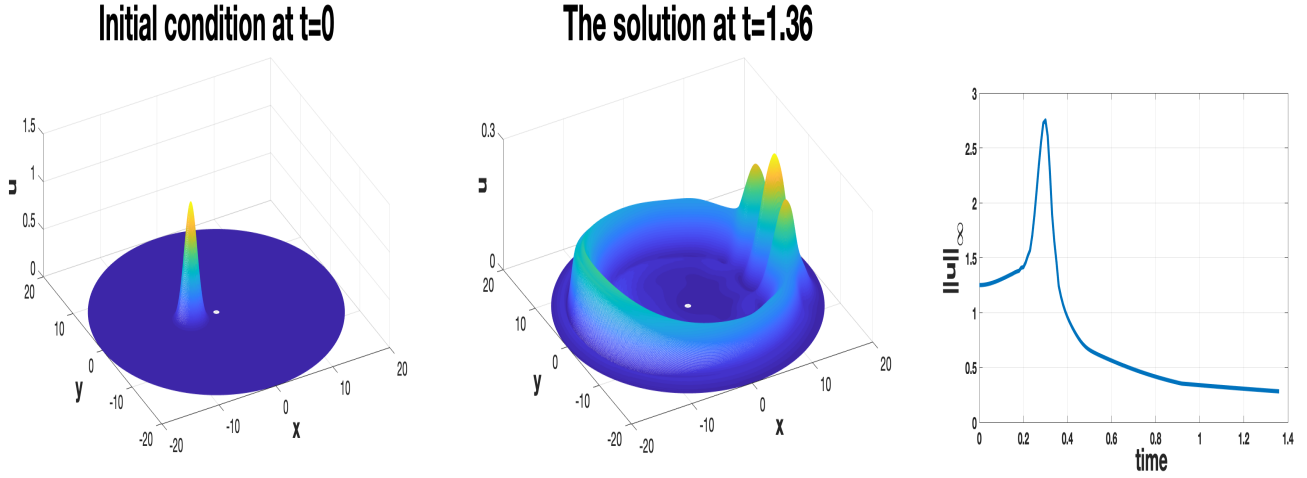
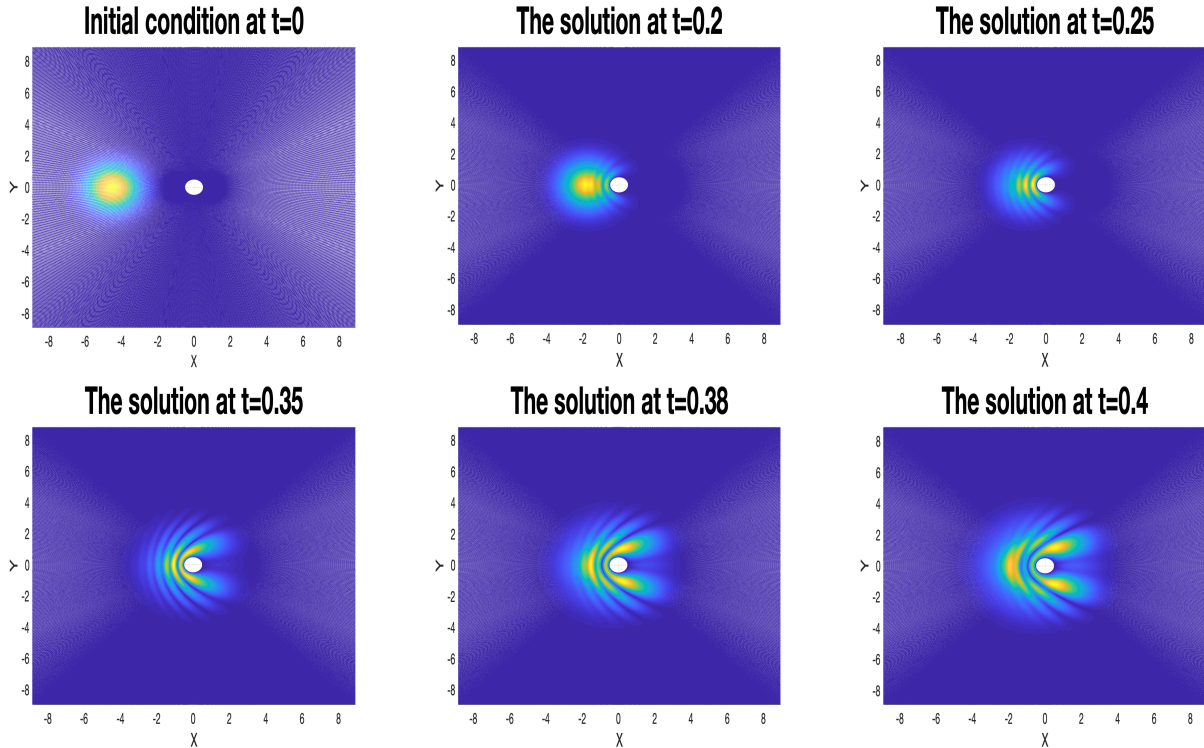


FIGURE 29. Solution $u(t)$ to the 2d quintic NLS $_{\Omega}$ equation with the initial condition u_0 from (2.2), $A_0 = 1.25$, $(x_c, y_c) = (-4.5, 0)$ and $v = (15, 0)$ (left), the solution $u(t)$ moving on the line $y = 0$ at time $t = 1.36$ (middle); time dependence of the L^{∞} -norm (right).

In this case, the solution scatters and does not preserve the shape of the original solitary wave. After the collision, the solitary wave solution forms two (then later possibly three, and eventually just one) bumps with a circular reflecting waves, part of which reflects backward, see Figure 30. We observe also that the leading reflected wave has a dispersive behavior. Moreover, one can see that the presence of the obstacle completely prevents blow-up. Before the interaction, the L^{∞} -norm of the solution starts increasing, indicating a possible blow-up behavior, however, after the interaction with the obstacle, the amplitude of the solution decreases toward 0, which confirms the dispersion of the solution in a long term, thus, scattering.



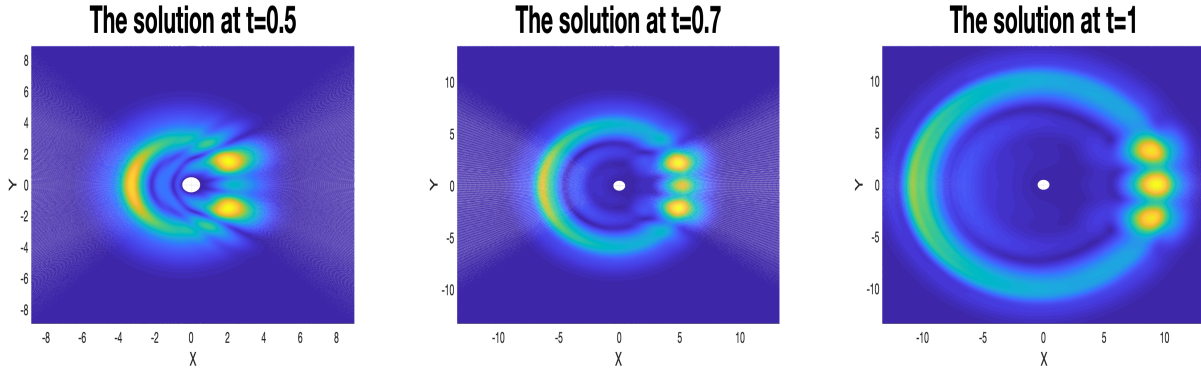


FIGURE 30. Snapshots of the behavior of the solution $u(t)$ to the 2d quintic NLS_Ω equation for different times in the strong interaction between the solution and the obstacle, with (x, y) -view.

8. DEPENDENCE ON THE OBSTACLE SIZE

In this section, we describe the behavior of the solution to the cubic and quintic NLS_Ω equations in the strong interaction case, as in Figures 24 and 28, depending on the size of the obstacle (a disk of radius r_*). We study the strong interaction of the solution with the obstacle in terms of the transmitted and the reflected parts of the mass: we call the transmitted mass $M_T[u^n]$, the discrete L^2 -norm of the solution u^n at time $t = t^n$ on the right-half plane

$$\Omega_+ := \{(r, \theta) \in [r_*, R] \times [0, 2\pi] : 0 \leq \theta \leq \frac{\pi}{2} \text{ and } \frac{3\pi}{2} \leq \theta \leq 2\pi\},$$

thus, we obtain the mass on the right-half plane $\{(x, y) \in \Omega : x \geq 0\}$,

$$M_T[u^n] = \sum_{k=0}^{N_r} \sum_{\substack{0 \leq j \leq \frac{\pi}{2} \\ \frac{3\pi}{2} \leq j \leq 2\pi}}^{N_\theta} |u_{k,j}^n|^2 r_k \Delta r \Delta \theta, \quad \text{for } n \geq 0.$$

We call the reflected mass $M_R[u^n]$, the discrete L^2 -norm of the solution u^n at time $t = t^n$ on the left-half plane

$$\Omega_- := \{(r, \theta) \in [r_*, R] \times [0, 2\pi] : \frac{\pi}{2} < \theta < \frac{3\pi}{2}\},$$

so that, we obtain the mass on the left-half plane $\{(x, y) \in \Omega : x \leq 0\}$,

$$M_R[u^n] = \sum_{k=0}^{N_r} \sum_{\frac{\pi}{2} < j < \frac{3\pi}{2}}^{N_\theta} |u_{k,j}^n|^2 r_k \Delta r \Delta \theta, \quad \text{for } n \geq 0.$$

We consider different values for the radius r_* of the obstacle and investigate solutions with initial data (2.2) having the amplitude A_0 and the velocity $v = (v_x, v_y)$. The spatial translation (x_c, y_c) in the initial data depends on the radius r_* of the obstacle so that the initial conditions would satisfy the Dirichlet boundary condition. In §8.1, we first study the cubic, L^2 -critical, NLS_Ω equation and in §8.2, we investigate the super-critical NLS_Ω equation.

8.1. The L^2 -critical case. We consider the cubic NLS_Ω equation with the initial condition as in (2.2) with the following parameters:

$$A_0 = 2.5, \quad v_x = 15, \quad v_y = 15, \quad x_c = -4 - r_*, \quad y_c = -4 - r_*. \quad (8.1)$$

The solution u moves on the line $y = x$, i.e., in the same direction as the outward normal vector of Ω . The dependence of the solution behavior on the obstacle size in the strong interaction case is as follows (the summary is given in Table 3):

- For $r_\star = 0.1$, the solution splits into two bumps with a *small* backward reflection, which has a dispersive behavior. As there is a sufficient mass transmitted, the two bumps get back together and behave as a single solitary wave, which blows up in finite time, see Figure 31.
- For $0.2 \leq r_\star \leq 0.4$, we observe that the solution splits into several bumps with a *small* reflected part that leads to some loss of the transmitted mass and results in an overall scattering behavior of the solution (the transmitted part reconstructs back into one bump).
- For $0.5 \leq r_\star \leq 0.7$, we observe that the solution splits into several *small* bumps, which later make up the transmitted part of the solution with an *important* reflected part. The solution has a similar behavior as in the previous case, however, the reflected mass is higher than the half of the total mass $\frac{1}{2}M[u_0] = 9.8175$, which endorses the dispersive (scattering) behavior of the solution.
- For $0.8 \leq r_\star < 3$, the interaction surface between the solution and the obstacle is sufficiently large, thus, the solution scatters: the main part of the solution is mostly reflected back with a small dispersive transmitted part. We observe a reverse behavior of the transmitted and the reflected part of the solution compared to case for $0.2 \leq r_\star \leq 0.4$, see Figure 32 (for an example with $r_\star = 2$).
- For $r_\star \geq 4$, the solution behaves quite different from the previous cases: the solution blows up in finite time at the boundary of the obstacle, as the interaction region is larger than the contour of the solution and there is almost no transmission of the solution (the transmitted mass is around 10^{-5}). The solution can not cross or get around the obstacle boundary, hence, the solution concentrates in its blow-up core at the obstacle's boundary, see Figure 33 (for an example with $r_\star = 5$).

r_\star	Discrete total mass	Behavior of the solution	Discrete reflected mass	Discrete transmitted mass
$r_\star = 0.1$	19.6350	Blow-up at $t \approx 0.888$	3.7746 at $t \approx 0.888$	15.8603 at $t \approx 0.888$
$r_\star = 0.2$	19.6350	Scattering	5.2641 at $t \approx 1.2$	14.3709 at $t \approx 1.2$
$r_\star = 0.3$	19.6350	Scattering	7.1144 at $t \approx 1.2$	12.5206 at $t \approx 1.2$
$r_\star = 0.4$	19.6350	Scattering	8.8085 at $t \approx 1.2$	10.8264 at $t \approx 1.2$
$r_\star = 0.5$	19.6350	Scattering	10.1753 at $t \approx 1.2$	9.4596 at $t \approx 1.2$
$r_\star = 0.6$	19.6350	Scattering	11.4460 at $t \approx 1.2$	8.1890 at $t \approx 1.2$
$r_\star = 0.7$	19.6350	Scattering	12.5008 at $t \approx 1.2$	7.1341 at $t \approx 1.2$
$r_\star = 0.8$	19.6350	Scattering	13.4017 at $t \approx 1.2$	6.2332 at $t \approx 1.2$
$r_\star = 0.9$	19.6350	Scattering	14.1658 at $t \approx 1.2$	5.4691 at $t \approx 1.2$
$r_\star = 1$	19.6350	Scattering	14.8208 at $t \approx 1.2$	4.8141 at $t \approx 1.2$
$r_\star = 2$	19.6350	Scattering	18.0537 at $t \approx 1.2$	1.5813 at $t \approx 1.2$
$r_\star = 3$	19.6350	Scattering	19.0024 at $t \approx 1.2$	0.6325 at $t \approx 1.2$
$r_\star = 4$	19.6350	Blow-up at $t \approx 0.36$	19.6349 at $t \approx 0.36$	$5.6838e - 05$ at $t \approx 0.36$
$r_\star = 5$	19.6350	Blow-up at $t \approx 0.36$	19.6349 at $t \approx 0.36$	$5.6838e - 05$ at $t \approx 0.36$

TABLE 3. Different obstacle size r_\star and the corresponding behavior of the solution $u(t)$ to the 2d cubic NLS $_\Omega$ equation with u_0 from (2.2) with (8.1) with the discrete total mass, reflected and transmitted discrete mass after interaction with the obstacle at time t .

Next, we give examples of the solution to the cubic NLS $_\Omega$ equation with a slightly smaller initial amplitude A_0 , depending on the size of the obstacle (the strong interaction case), see Figure 24. We consider the initial condition (2.2), with the following parameters:

$$A_0 = 2.25, \quad v_x = 15, \quad v_y = 15, \quad x_c = -4 - r_\star \quad \text{and} \quad y_c = -4 - r_\star. \quad (8.2)$$

We record all observations in this case in Table 4.

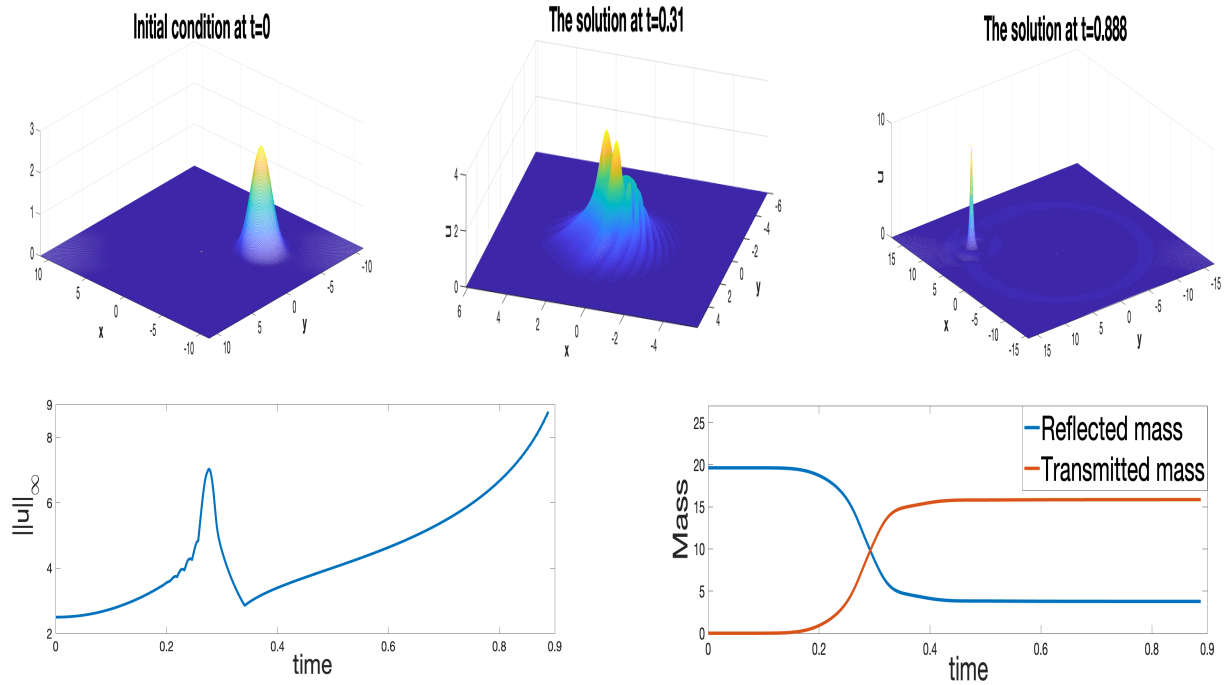


FIGURE 31. Solution to the $2d$ cubic NLS_{Ω} equation with the radius of the obstacle $r_{\star} = 0.1$ and u_0 from (2.2) with (8.1) moving along the line $y = x$. Snapshots of the blow-up solution $u(t)$ at $t = 0$ (top left), $t = 0.31$ (middle top) and $t = 0.888$ (top right). Time dependence of the L^{∞} -norm (bottom left) and of the transmitted and the reflected mass (bottom right).

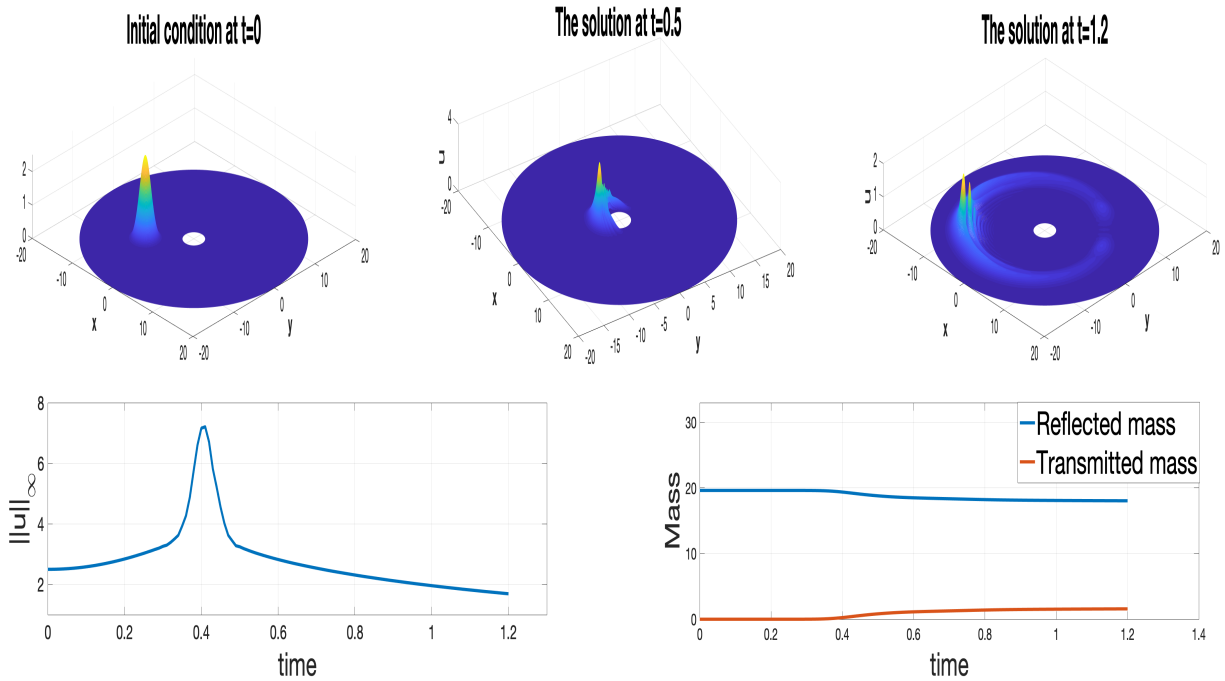


FIGURE 32. Solution to the $2d$ cubic NLS_{Ω} equation with the obstacle radius $r_{\star} = 2$ and u_0 from (2.2) with (8.1) moving along the line $y = x$. Snapshots of the scattering solution $u(t)$ at $t = 0$ (top left), $t = 0.5$ (middle top) and $t = 1.2$ (top right). Time dependence of the L^{∞} -norm (bottom left) and of the transmitted and the reflected mass (bottom right).

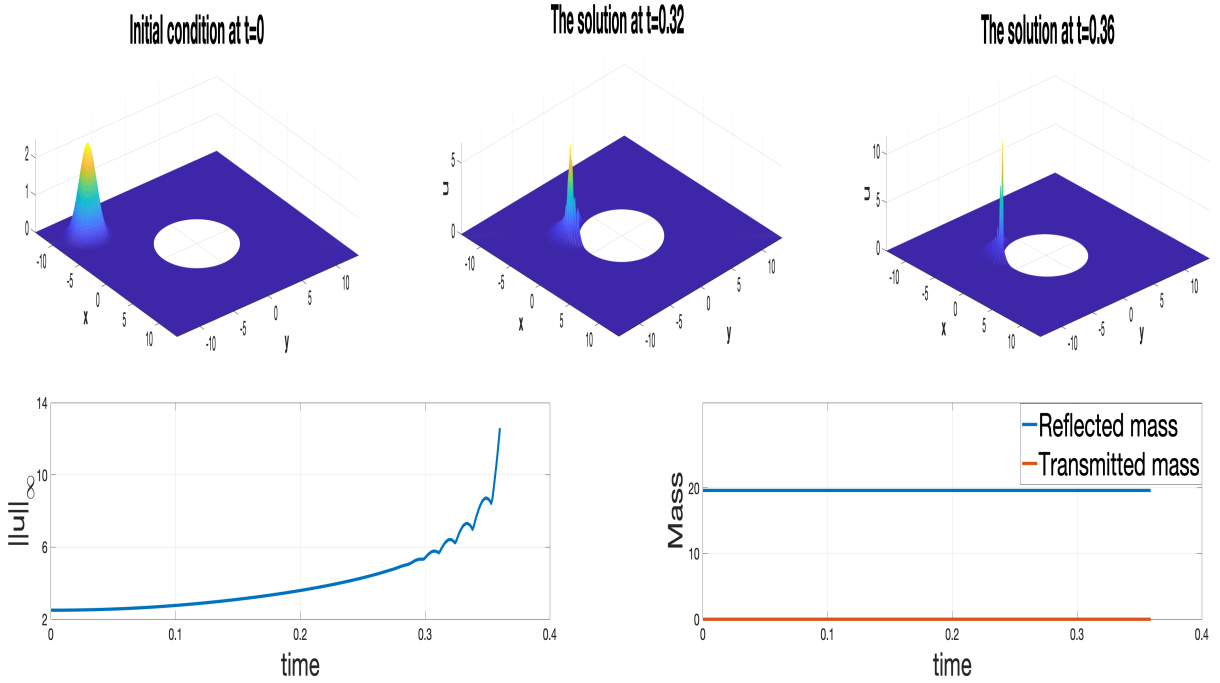


FIGURE 33. Solution to the $2d$ cubic NLS_{Ω} equation with the obstacle radius $r_{\star} = 5$ and u_0 from (2.2) with (8.1) moving along the line $y = x$. Snapshots of the blow-up solution $u(t)$ at $t = 0$ (top left), $t = 0.32$ (middle top) and $t = 0.36$ (top right). Time dependence of the L^{∞} -norm (bottom left) and of the transmitted and the reflected mass (bottom right).

r_{\star}	Discrete total mass	Behavior of the solution	Discrete reflected mass	Discrete transmitted mass
$r_{\star} = 0.1$	15.9043	Blow-up at $t \approx 0.891$	2.448 at $t \approx 0.891$	13.4563 at $t \approx 0.891$
$r_{\star} = 0.2$	15.9043	Scattering	3.684 at $t \approx 1.2$	12.2203 at $t \approx 1.2$
$r_{\star} = 0.3$	15.9043	Scattering	5.0335 at $t \approx 1.2$	10.8708 at $t \approx 1.2$
$r_{\star} = 0.4$	15.9043	Scattering	6.3137 at $t \approx 1.2$	9.5906 at $t \approx 1.2$
$r_{\star} = 0.5$	15.9043	Scattering	7.4179 at $t \approx 1.2$	8.4864 at $t \approx 1.2$
$r_{\star} = 0.6$	15.9043	Scattering	8.3902 at $t \approx 1.2$	7.5141 at $t \approx 1.2$
$r_{\star} = 0.7$	15.9043	Scattering	9.2624 at $t \approx 1.2$	6.6419 at $t \approx 1.2$
$r_{\star} = 0.8$	15.9043	Scattering	10.0278 at $t \approx 1.2$	5.8765 at $t \approx 1.2$
$r_{\star} = 0.9$	15.90430	Scattering	10.6936 at $t \approx 1.2$	5.2107 at $t \approx 1.2$
$r_{\star} = 1$	15.9043	Scattering	11.2791 at $t \approx 1.2$	4.6253 at $t \approx 1.2$
$r_{\star} = 2$	15.9043	Scattering	14.3843 at $t \approx 1.2$	1.52 at $t \approx 1.2$
$r_{\star} = 3$	15.9043	Scattering	15.3338 at $t \approx 1.2$	0.57049 at $t \approx 1.2$
$r_{\star} = 4$	15.9043	Scattering	15.65 at $t \approx 1.2$	0.2543 at $t \approx 1.2$
$r_{\star} = 5$	15.9043	Blow-up at $t \approx 0.754$	15.8291 at $t \approx 0.36$	0.07523 at $t \approx 0.36$
$r_{\star} = 6$	15.9043	Blow-up at $t \approx 0.754$	15.8291 at $t \approx 0.36$	0.07523 at $t \approx 0.36$

TABLE 4. Influence of the obstacle radius r_{\star} onto the behavior of the solution $u(t)$ to the $2d$ cubic NLS_{Ω} equation with u_0 from (2.2) and (8.2) with the (initial) discrete total mass, and after the interaction the reflected and transmitted discrete mass parts at time t .

We observe that in the case $r_{\star} = 0.1$, in both examples (8.1) and (8.2) with $A_0 = 2.25$ and $A_0 = 2.5$, the solutions blow up in finite time, as the reflection parts of the respective solutions are small and almost all of the solution is transmitted. The time evolution proceeds as follows First, the solution hugs around the obstacle, splitting into two bumps and then, since the radius of the obstacle is small, the solution gets back together to form a single bump in a few time steps. One can observe that the solution has a substantial

transmitted mass, which leads to a blow up in finite time. It seems as the solitary bump has a similar shape of the solution as if there would be no obstacle interaction near the blow-up time, in particular, it would be interesting to investigate the profile and other features of the blow-up solution after the interaction with the obstacle). As the radius of the obstacle increases, we see very different dynamics of the solution compared to the NLS $_{\mathbb{R}^2}$ equation in the whole space, since this solution blows up in finite time when the obstacle is absent (or has a very small radius).

8.2. The L^2 -supercritical case. In this section, we summarize the behavior of the solution to the quintic NLS $_{\Omega}$ equation depending on the radius r_{\star} of the obstacle and we study the strong interaction. As before, we take a set of values of the obstacle radius r_{\star} and investigate the behavior of the solution moving on the line $y = 0$ (in the strong interaction case) as shown in Figure 28.

We take the initial data as in (2.2) and fix the following parameters:

$$A_0 = 1.25, \quad v_x = 15, \quad v_y = 0, \quad x_c = -4 - r_{\star} \text{ and } y_c = 0. \quad (8.3)$$

We first discuss behavior of solutions for different sized of the obstacle, specifically, we show the snapshots of the time evolution of the above data for the obstacle radii $r_{\star} = 0.1$, $r_{\star} = 1$ and $r_{\star} = 3$. Then we provide the summary of results in Table 5.

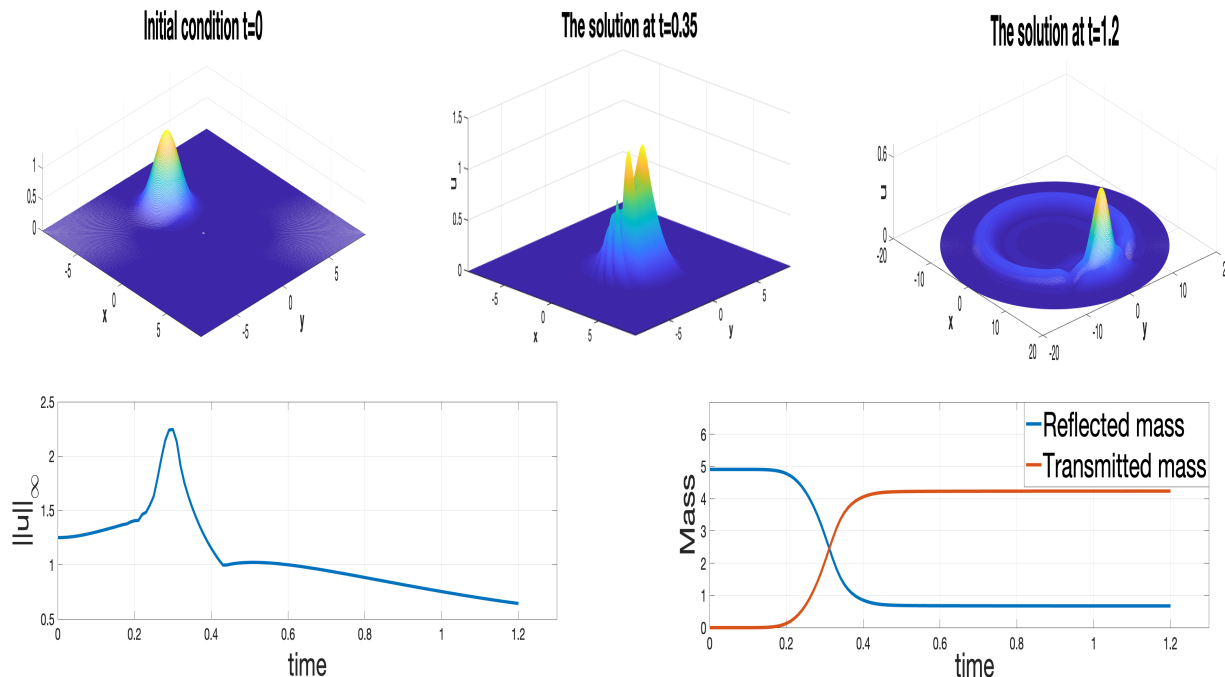


FIGURE 34. Solution to the 2d quintic NLS $_{\Omega}$ equation with the obstacle radius $r_{\star} = 0.1$ and u_0 from (2.2) with (8.3) moving along the line $y = 0$. Snapshots of the scattering solution $u(t)$ at $t = 0$ (top left), $t = 0.35$ (middle top) and $t = 1.2$ (top right). Time dependence of the L^{∞} -norm (bottom left) and of the transmitted and the reflected mass (bottom right).

We observe that even for a small obstacle, $r_{\star} = 0.1$, the solution scatters with a small backward reflection, see Figure 34. For $r_{\star} = 1$ the solution has a similar dispersive behavior as in the previous examples, however, we note that the reflected backward part is more relevant and important, which ensures the dispersive behavior of the solutions, see Figure 35. On the other hand, for $r_{\star} = 3$ the solution has a different behavior: the solution blows up in finite time at the boundary of the obstacle, as the interaction region becomes larger than the solution contour, and thus, the solution can not be transmitted around the obstacle. It concentrates

at its blow-up core at the obstacle's boundary, see Figure 36.

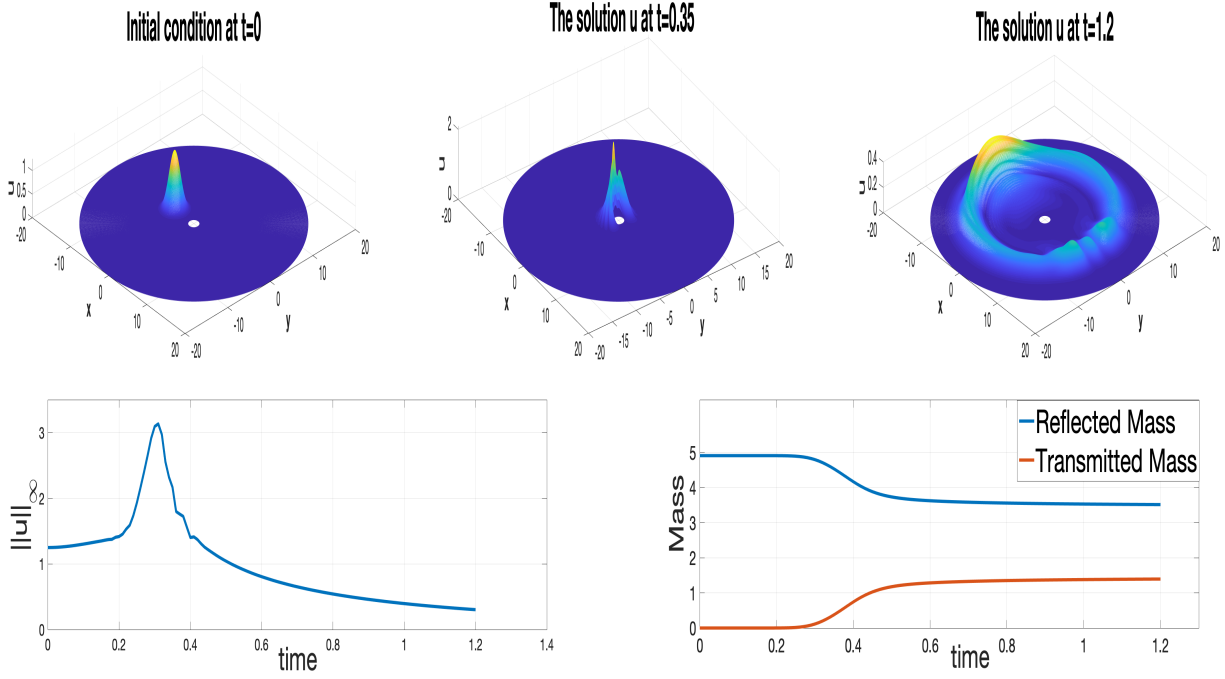


FIGURE 35. Solution to the 2d quintic NLS_{Ω} equation with the obstacle radius $r_{\star} = 1$ and u_0 from (2.2) and (8.3) moving along the line $y = 0$. Snapshots of the scattering solution $u(t)$ at $t = 0$ (top left), $t = 0.35$ (middle top) and $t = 1.2$ (top right). Time dependence of the L^{∞} -norm (bottom left) and of the transmitted and the reflected mass (bottom right).

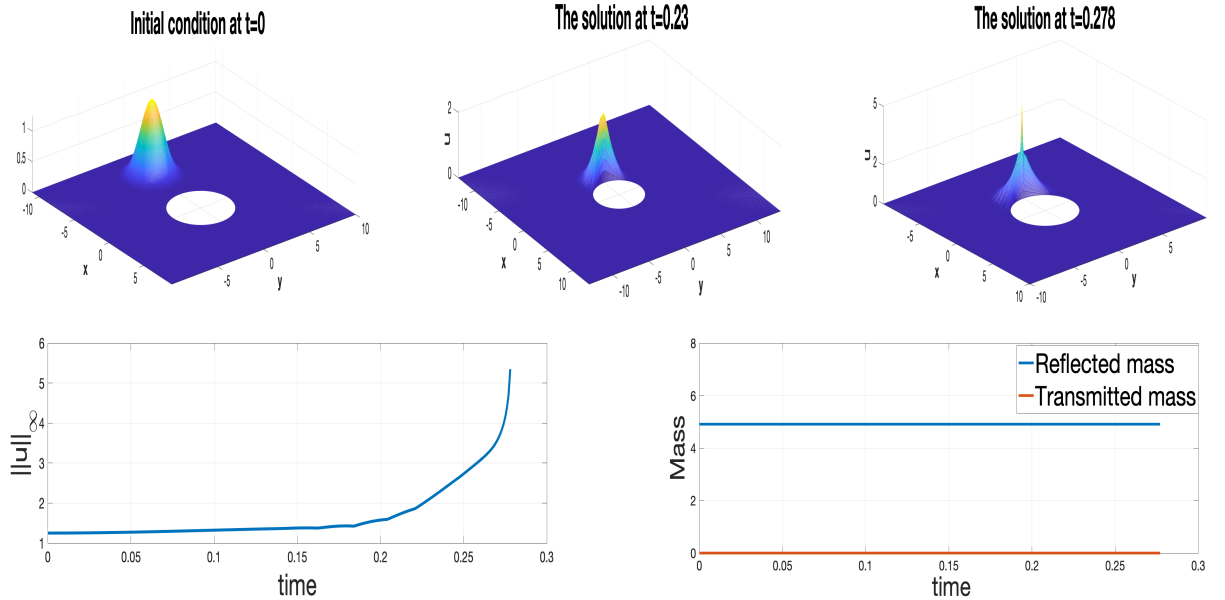


FIGURE 36. Solution to the 2d quintic NLS_{Ω} equation with the obstacle radius $r_{\star} = 3$ and u_0 from (2.2) with (8.3) moving along the line $y = 0$. Snapshots of the blow-up solution $u(t)$ at $t = 0$ (top left), $t = 0.23$ (middle top) and $t = 0.278$ (top right). Time dependence of the L^{∞} -norm (bottom left) and of the transmitted and the reflected mass (bottom right).

r_*	Discrete total mass	Behavior of the solution	Discrete reflected mass	Discrete transmitted mass
$r_* = 0.1$	4.9087	Scattering	0.67277 at $t \approx 1.2$	4.236 at $t \approx 1.2$
$r_* = 0.2$	4.9087	Scattering	1.1094 at $t \approx 1.2$	3.7994 at $t \approx 1.2$
$r_* = 0.3$	4.9087	Scattering	1.5618 at $t \approx 1.2$	3.3469 at $t \approx 1.2$
$r_* = 0.4$	4.9087	Scattering	1.9578 at $t \approx 1.2$	2.9509 at $t \approx 1.2$
$r_* = 0.5$	4.9087	Scattering	2.3141 at $t \approx 1.2$	2.5946 at $t \approx 1.2$
$r_* = 0.6$	4.9087	Scattering	2.6199 at $t \approx 1.2$	2.2888 at $t \approx 1.2$
$r_* = 0.7$	4.9087	Scattering	2.8845 at $t \approx 1.2$	2.0243 at $t \approx 1.2$
$r_* = 0.8$	4.9087	Scattering	3.1181 at $t \approx 1.2$	1.7906 at $t \approx 1.2$
$r_* = 0.9$	4.9087	Scattering	3.3263 at $t \approx 1.2$	1.5824 at $t \approx 1.2$
$r_* = 1$	4.9087	Scattering	3.5143 at $t \approx 1.2$	1.3945 at $t \approx 1.2$
$r_* = 1.5$	4.9087	Blow up at $t \approx 0.377$	4.7085 at $t \approx 0.377$	0.20019 at $t \approx 0.377$
$r_* = 2$	4.9087	Blow up at $t \approx 0.285$	4.908 at $t \approx 0.285$	$7.5778e^{-4}$ at $t \approx 0.285$
$r_* = 3$	4.9087	Blow up at $t \approx 0.278$	4.9087 at $t \approx 0.278$	$6.2761e^{-8}$ at $t \approx 0.278$

TABLE 5. Influence of the obstacle size r_* onto the behavior of the solution $u(t)$ to the $2d$ quintic NLS $_{\Omega}$ equation with u_0 from (2.2) and (8.3) with the discrete total mass, reflected and transmitted discrete mass parts after interaction with the obstacle at time t .

9. BLOW-UP: WALL-TYPE INITIAL DATA

In this section we study blow-up solutions in the strong interaction case (moving directly towards the obstacle as shown in Figure 28) for the large obstacle size and, in some cases, reuniting back into one single bump, which then blows up. We investigate the behavior of solutions to the cubic NLS $_{\Omega}$ equation with a special round Wall-type super-Gaussian initial data. We consider the initial condition, which is defined by the product of a phase in terms of the angle $\Theta := (\Theta_j)_{1 \leq j \leq N}$ with a super-Gaussian in terms of $r := (r_i)_{1 \leq i \leq N}$:

$$u_0(r, \Theta) := A_0 \left(e^{-(r+r_c)^4} \times e^{-\frac{1}{2}(\Theta-\pi)^4} \right) e^{i(\frac{1}{2}(v_x r \cos(\Theta) + v_y r \sin(\Theta)))}, \quad (9.1)$$

where

$$A_0 = 2.5, \quad v_x = 15, \quad v_y = 0, \quad \text{and} \quad r_c = -4 - r_*. \quad (9.2)$$

Note that, due to the construction of this solution, the L^2 -norm, or the mass, of u_0 depends on the radius of the obstacle r_* , i.e., the mass increases as r_* becomes larger. This does not affect the conservation of the mass throughout the simulation for fixed r_* . In the following simulations, we consider $r_* = 3$ (Figure 37)

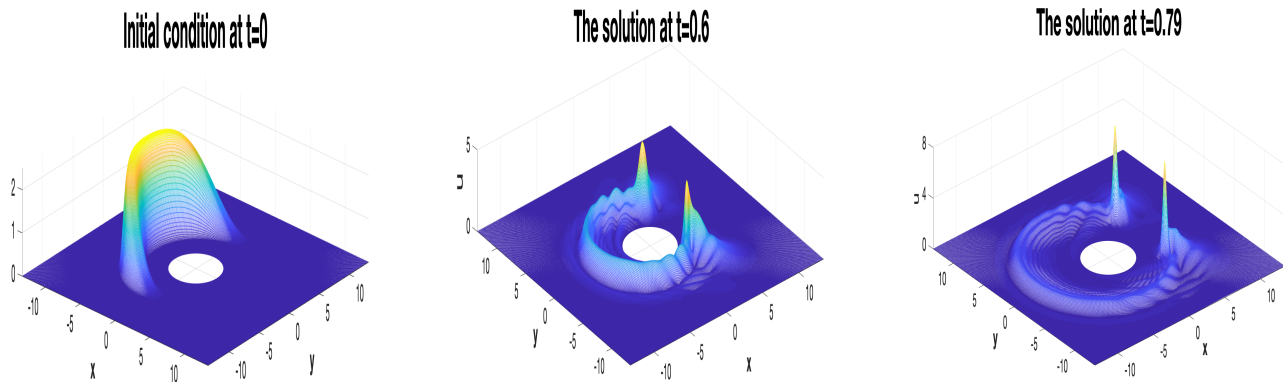


FIGURE 37. Solution to the $2d$ cubic NLS $_{\Omega}$ equation with the obstacle radius $r_* = 3$ and u_0 from (9.1) with (9.2) moving along the line $y = 0$. Snapshots of the blow-up solution $u(t)$ at $t = 0$ (left), $t = 0.6$ (middle) and $t = 0.79$ (right).

and $r_\star = 5$ (Figure 39). We observe that even with the large radius of the obstacle, the solution blows up in finite time. After the interaction, the solution splits into two bumps, with an essential backward reflection and a substantial transmitted mass. Before the two bumps could merge together, they concentrate in their own blow-up core regions, that is, each bump blows up separately at a single point location, see the right plots in Figure 37 for $r_\star = 3$ and Figure 39 for $r_\star = 5$; also the growth of the L^∞ norm on the right plots of Figures 38 and 40.

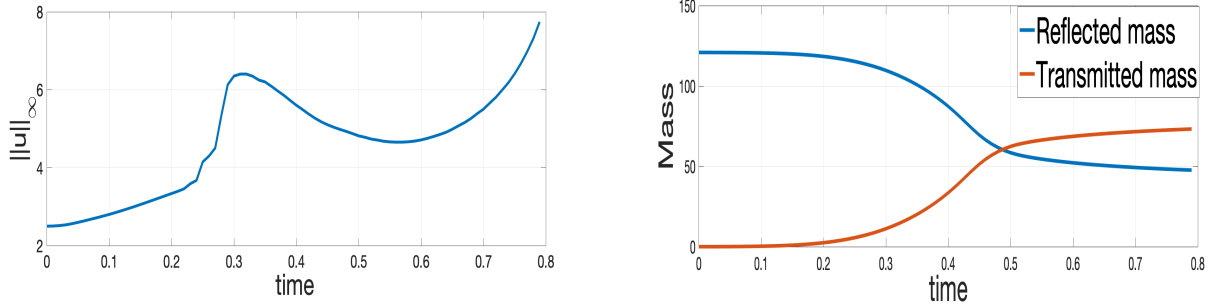


FIGURE 38. Time dependence of the L^∞ -norm (left) and of the transmitted and the reflected mass (right) for the solution in Figure 37.

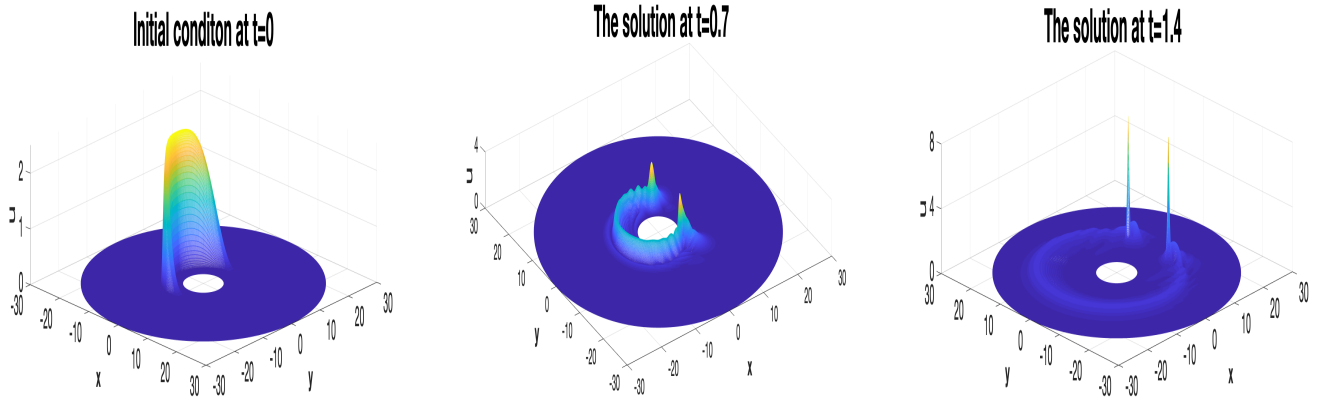


FIGURE 39. Solution to the 2d cubic NLS $_\Omega$ equation with the radius of the obstacle $r_\star = 5$ and u_0 from (9.1) with (9.2) moving along the line $y = 0$. Snapshots of the blow-up solution $u(t)$ at $t = 0$ (left), $t = 0.7$ (top) and $t = 1.4$ (right).

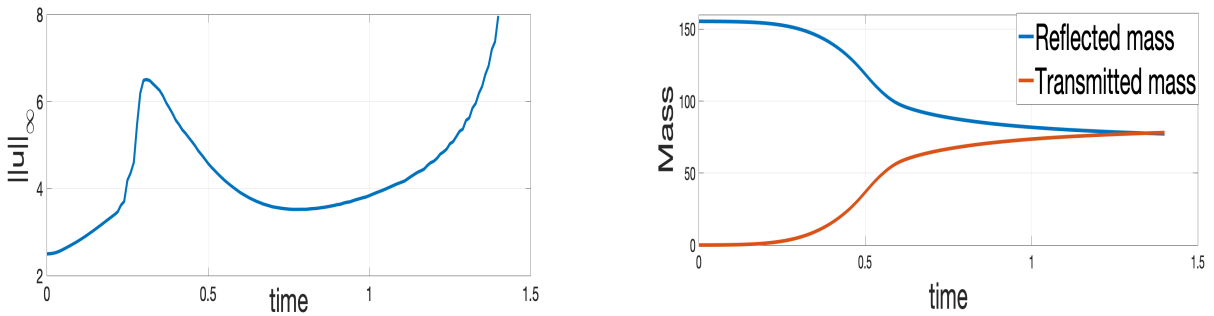


FIGURE 40. Time dependence of the L^∞ -norm (left) and of the transmitted and the reflected mass (right) for the solution in Figure 39.

We next consider the data (9.1) with the following parameters (changing the amplitude):

$$A_0 = 1.5, \quad v_x = 15, \quad v_y = 0, \quad \text{and } r_c = -4 - r_\star. \quad (9.3)$$

For the last two examples in this paper, we consider $r_\star = 2$ and $r_\star = 10$ with the data in (9.3).

First, we observe that the solution blows up in finite time even if the radius of the obstacle is large (compared to the previous example with the amplitude $A_0 = 2.5$), see Figure 41, where $r_\star = 2$.

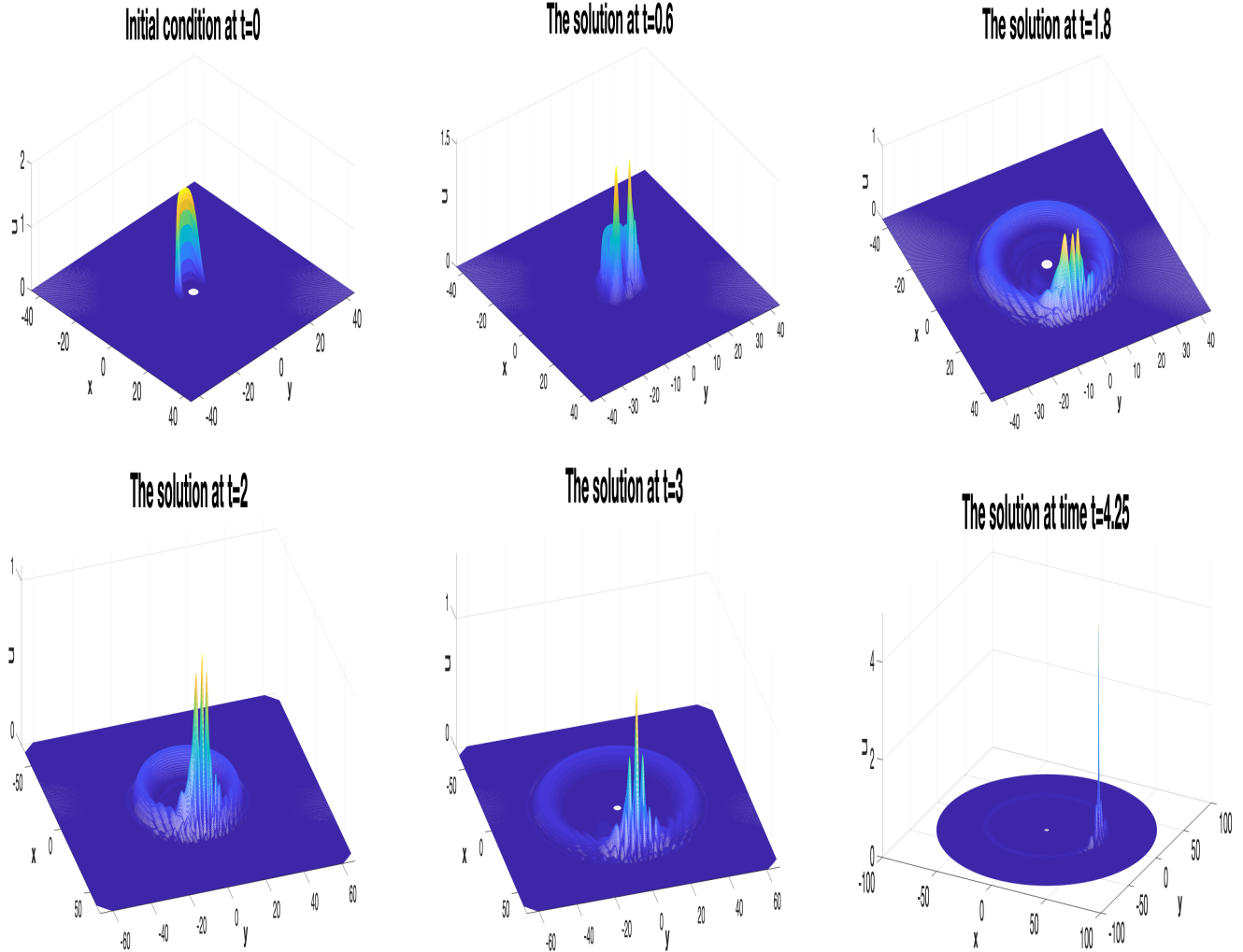


FIGURE 41. Solution to the $2d$ cubic NLS_Ω equation with the obstacle radius $r_\star = 2$ and u_0 from (9.1) with (9.3), moving along the line $y = 0$. Snapshots of the blow-up solution $u(t)$ at $t = 0, 0.6, 1.8$ (top row), $t = 2, 3, 4.25$ (bottom row).

After the interaction, the solution splits into two bumps, with the backward reflection having a substantial amount of the transmitted mass. Then the two bumps have sufficient time to merge together and pump the mass from both lumps (as the circle expands) into a single bump, which has enough mass to concentrate in its core to blow up in finite time, see Figure 41 and also the L^∞ norm together with the change in time in the transmitted and reflected mass in Figure 42.

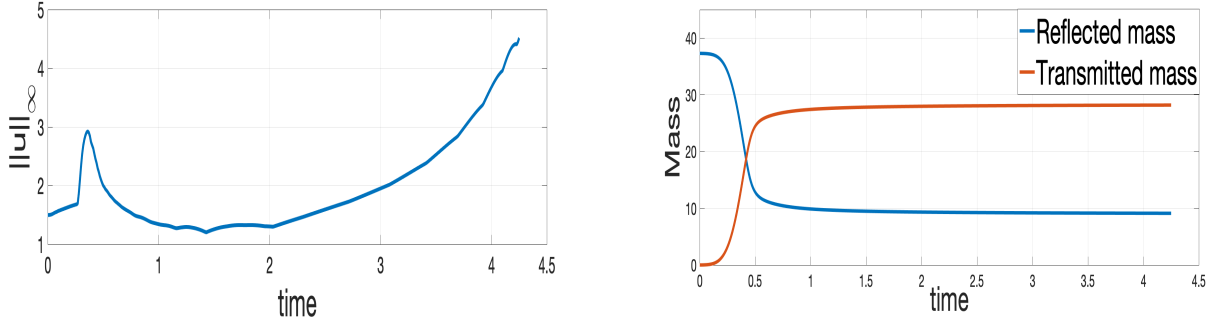


FIGURE 42. Time dependence of the L^∞ -norm (left) and of the transmitted and the reflected mass (right) for the solution in Figure 41.

However, for a larger radius, for example $r_\star \geq 3$, the solution has to hug around an obstacle with the bigger size, and thus, the mass gets dispersed more around, hence, less of the mass is transmitted, which concludes in the overall scattering behavior. See Figure 43 for an example of the obstacle size $r_\star = 10$.

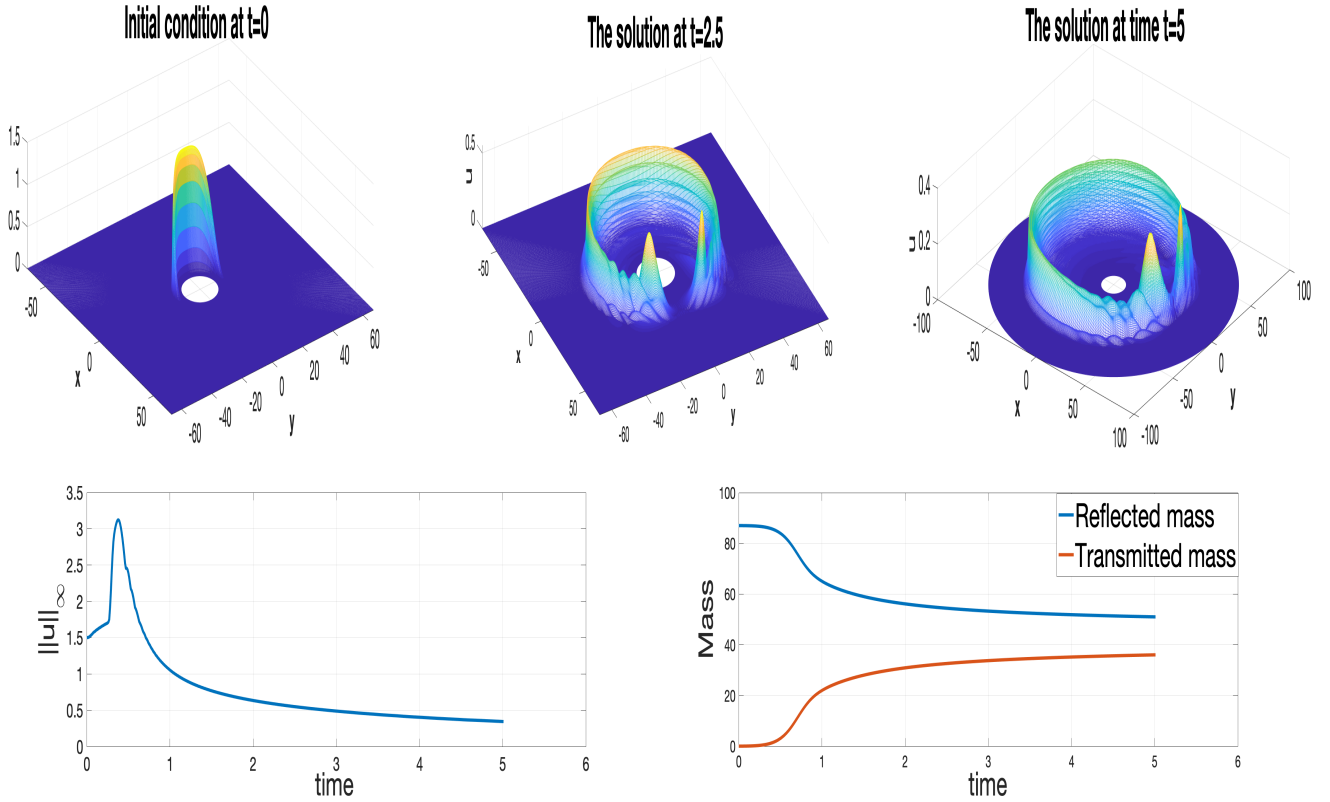


FIGURE 43. Solution to the 2d cubic NLS_Ω equation with the radius of the obstacle $r_\star = 10$ and u_0 from (9.1) with (9.3). Snapshots of the scattering solution $u(t)$ at $t = 0$ (top left), $t = 2.5$ (middle top) and $t = 5$ (top right). Time dependence of the L^∞ -norm (bottom left) and of the transmitted and the reflected mass (bottom right).

For the initial data (9.3) to track the dependence as the radius of the obstacle increases we perform numerical simulations for a variety of radii and provide the summary of the results in Table 6.

r_*	Discrete total mass	Behavior of the solution	Discrete reflected mass	Discrete transmitted mass
$r_* = 0.1$	25.4924	Blow up at $t \approx 1.54$	0.70785 at $t \approx 1.54$	24.7846 at $t \approx 1.54$
$r_* = 0.5$	27.9795	Blow up at $t \approx 1.75$	2.4016 at $t \approx 1.75$	25.5779 at $t \approx 1.75$
$r_* = 1$	31.0883	Blow up at $t \approx 2.4$	4.6621 at $t \approx 2.4$	26.4262 at $t \approx 2.4$
$r_* = 1.5$	34.1971	Blow up at $t \approx 3.174$	6.8188 at $t \approx 3.174$	27.3784 at $t \approx 3.174$
$r_* = 2$	37.3060	Blow up at $t \approx 4.25$	9.1169 at $t \approx 4.25$	28.1891 at $t \approx 4.25$
$r_* = 3$	43.5236	Scattering	14.2976 at $t \approx 6$	29.226 at $t \approx 6$
$r_* = 4$	49.7413	Scattering	19.0758 at $t \approx 6$	30.6655 at $t \approx 6$
$r_* = 5$	55.9590	Scattering	23.3673 at $t \approx 5$	32.5917 at $t \approx 5$
$r_* = 10$	87.0473	Scattering	36.0356 at $t \approx 5$	51.0117 at $t \approx 5$

TABLE 6. Influence of the obstacle size r_* onto the behavior of the solution $u(t)$ to the $2d$ cubic NLS $_{\Omega}$ equation with u_0 from (9.1) and (9.3), with the (initial) discrete total mass, after the interaction the reflected and transmitted discrete mass parts at time t .

10. CONCLUSION

In this work we initiated a numerical study of how the behavior of solutions can change in a presence of a smooth convex obstacle. We observe that the interaction between a solitary wave and the obstacle can significantly influence the overall behavior of the solution to the NLS $_{\Omega}$ equation, which depends on the direction of the velocity vector $\vec{v} = (v_x, v_y)$, the size of the obstacle (radius r_*), the initial distance (d vs. d^*) to the obstacle and the translation parameters (x_c, y_c) . The presence of the obstacle yields strong, weak or no interaction. We observed in Sections 6.1 and 6.2 that even a small interaction between the obstacle and a single peak solution has some influence on the dynamics (at the least, on the blow-up time). Moreover, we conclude that the strong interaction has a significant effect on the behavior of solutions depending on the size of the obstacle, for example, instead of approaching a solitary wave solution with a single bump, the shape of the solution drastically changes after the collision, splitting it into several bumps with a backward reflected wave. The appearance of the reflection waves due to the presence of the obstacle with Dirichlet boundary conditions prevents the solution from blowing up in finite time in some cases. Furthermore, this backward reflection has always a dispersive character, this might be the reason why the solution scatters in most of the cases after a strong interaction. However, if the obstacle is very small or if the contour of the solution is significantly bigger than the radius of the obstacle, we observed the existence of blow-up solutions. In this case, the interaction surface is negligible so that the mass of the solution is almost all transmitted, which is sufficient to develop a blow-up. If the obstacle is large enough or if there is no transmission of the solution, then, either the solution is completely reflected back or the solution concentrates in its blow-up core at the obstacle's boundary, since the interaction region is relevant and it is larger than the contour of the solution. Furthermore, we construct new (*Wall-type*) initial condition, time evolution of which is characterized by its high mass transmission after a strong interaction, and then blowing up in finite time in a single point or in two separate locations (single points) after the strong interaction. For a weak interaction, i.e., when the solution preserves the shape as a traveling solitary wave, the solution behaves either as a solitary wave solution, constructed in [32] (which exists for all positive times), or as the one shown in [31] (see also [30]), a finite time (single point) blow-up solution (as if there would be no obstacle).

REFERENCES

- [1] AKRIVIS, G., DOUGALIS, V. A., AND KARAKASHIAN, O. Solving the systems of equations arising in the discretization of some nonlinear PDE's by implicit Runge-Kutta methods. *RAIRO Modél. Math. Anal. Numér.* 31, 2 (1997), 251–287.
- [2] AKRIVIS, G. D. Finite difference discretization of the cubic Schrödinger equation. *IMA J. Numer. Anal.* 13, 1 (1993), 115–124.

- [3] ANTON, R. Global existence for defocusing cubic NLS and Gross-Pitaevskii equations in three dimensional exterior domains. *J. Math. Pures Appl. (9)* 89, 4 (2008), 335–354.
- [4] BERESTYCKI, H., AND LIONS, P.-L. Nonlinear scalar field equations. I. Existence of a ground state. *Arch. Rational Mech. Anal.* 82, 4 (1983), 313–345.
- [5] BESSE, C. Schéma de relaxation pour l'équation de Schrödinger non linéaire et les systèmes de Davey et Stewartson. *C. R. Acad. Sci. Paris Sér. I Math.* 326, 12 (1998), 1427–1432.
- [6] BESSE, C. A relaxation scheme for the nonlinear Schrödinger equation. *SIAM J. Numer. Anal.* 42, 3 (2004), 934–952.
- [7] BESSE, C., BIDÉGARAY, B., AND DESCOMBES, S. Order estimates in time of splitting methods for the nonlinear Schrödinger equation. *SIAM J. Numer. Anal.* 40, 1 (2002), 26–40.
- [8] BLAIR, M. D., SMITH, H. F., AND SOGGE, C. D. Strichartz estimates and the nonlinear Schrödinger equation on manifolds with boundary. *Math. Ann.* 354, 4 (2012), 1397–1430.
- [9] BURQ, N., GÉRARD, P., AND TZVETKOV, N. On nonlinear Schrödinger equations in exterior domains. *Ann. Inst. H. Poincaré Anal. Non Linéaire* 21, 3 (2004), 295–318.
- [10] COFFMAN, C. V. Uniqueness of the ground state solution for $\Delta u - u + u^3 = 0$ and a variational characterization of other solutions. *Arch. Ration. Mech. Anal.* 46 (1972), 81–95.
- [11] COOPER, J., AND STRAUSS, W. A. Energy boundedness and decay of waves reflecting off a moving obstacle. *Indiana Univ. Math. J.* 25, 7 (1976), 671–690.
- [12] DELFOUR, M., FORTIN, M., AND PAYRE, G. Finite-difference solutions of a nonlinear Schrödinger equation. *J. Comput. Phys.* 44, 2 (1981), 277–288.
- [13] DODSON, B. Global well-posedness and scattering for the mass critical nonlinear Schrödinger equation with mass below the mass of the ground state. *Adv. Math.* 285 (2015), 1589–1618.
- [14] DUICKAERTS, T., HOLMER, J., AND ROUDENKO, S. Scattering for the non-radial 3D cubic nonlinear Schrödinger equation. *Math. Res. Lett.* 15, 6 (2008), 1233–1250.
- [15] DUICKAERTS, T., LANDOULSI, O., AND ROUDENKO, S. Threshold solutions for the focusing 3d cubic Schrödinger equation in the exterior of strictly convex obstacle. *J. Funct. Anal. forthcoming* (2020), arXiv:2010.07724.
- [16] DUICKAERTS, T., AND ROUDENKO, S. Threshold solutions for the focusing 3d cubic Schrödinger equation. *Rev. Mat. Iberoam.* 26, 1 (2010), 1–56.
- [17] FANG, D., XIE, J., AND CAZENAVE, T. Scattering for the focusing energy-subcritical nonlinear Schrödinger equation. *Sci. China Math.* 54, 10 (2011), 2037–2062.
- [18] GIDAS, B., NI, W. M., AND NIRENBERG, L. Symmetry of positive solutions of nonlinear elliptic equations in \mathbf{R}^n . In *Math. Analysis and Applications, Part A*, vol. 7 of *Adv. in Math. Suppl. Stud.* Academic Press, New York, 1981, pp. 369–402.
- [19] GUEVARA, C. D. Global behavior of finite energy solutions to the d -dimensional focusing nonlinear Schrödinger equation. *Appl. Math. Res. Express. AMRX*, 2 (2014), 177–243.
- [20] HOLMER, J., PLATTE, R., AND ROUDENKO, S. Blow-up criteria for the 3D cubic nonlinear Schrödinger equation. *Nonlinearity* 23, 4 (2010), 977–1030.
- [21] HOLMER, J., AND ROUDENKO, S. A sharp condition for scattering of the radial 3D cubic nonlinear Schrödinger equation. *Comm. Math. Phys.* 282, 2 (2008), 435–467.
- [22] IVANOVICI, O. Precised smoothing effect in the exterior of balls. *Asymptot. Anal.* 53, 4 (2007), 189–208.
- [23] IVANOVICI, O. On the Schrödinger equation outside strictly convex obstacles. *Analysis & PDE* 3, 3 (2010), 261–293.
- [24] IVANOVICI, O., AND PLANCHON, F. On the energy critical Schrödinger equation in 3D non-trapping domains. *Ann. Inst. H. Poincaré Anal. Non Linéaire* 27, 5 (2010), 1153–1177.
- [25] IVRIĬ, V. J. Exponential decay of the solution of the wave equation outside an almost star-shaped region. *Dokl. Akad. Nauk SSSR* 189 (1969), 938–940.
- [26] KARAKASHIAN, O., AKRIVIS, G. D., AND DOUGALIS, V. A. On optimal order error estimates for the nonlinear Schrödinger equation. *SIAM J. Numer. Anal.* 30, 2 (1993), 377–400.
- [27] KILLIP, R., VISAN, M., AND ZHANG, X. Riesz transforms outside a convex obstacle. *Internat. Math. Res. Not.* 2016, 19 (2015), 5875–5921.
- [28] KILLIP, R., VISAN, M., AND ZHANG, X. The focusing cubic NLS on exterior domains in three dimensions. *Appl. Math. Res. Express. AMRX*, 1 (2016), 146–180.
- [29] KWONG, M. K. Uniqueness of positive solutions of $\Delta u - u + u^p = 0$ in \mathbf{R}^n . *Arch. Rational Mech. Anal.* 105, 3 (1989), 243–266.
- [30] LANDOULSI, O. *Dynamics of the nonlinear focusing Schrödinger equation outside of a smooth, compact and convex obstacle.* PhD thesis, University Sorbonne Paris Nord, 2020.
- [31] LANDOULSI, O. On blow-up solutions of the nonlinear Schrödinger equation in the exterior of a convex obstacle. *preprint* (2020), arXiv:2012.13335.

- [32] LANDOULSI, O. Construction of a solitary wave solution of the nonlinear focusing Schrödinger equation outside a strictly convex obstacle in the L^2 -supercritical case. *Discrete Contin. Dyn. Syst.* 41, 2 (2021), 701–746.
- [33] LAX, P. D., MORAWETZ, C. S., AND PHILLIPS, R. S. The exponential decay of solutions of the wave equation in the exterior of a star-shaped obstacle. *Bull. Amer. Math. Soc.* 68 (1962), 593–595.
- [34] LAX, P. D., MORAWETZ, C. S., AND PHILLIPS, R. S. Exponential decay of solutions of the wave equation in the exterior of a star-shaped obstacle. *Comm. Pure Appl. Math.* 16 (1963), 477–486.
- [35] MORAWETZ, C. S. The decay of solutions of the exterior initial-boundary value problem for the wave equation. *Comm. Pure Appl. Math.* 14 (1961), 561–568.
- [36] MORAWETZ, C. S. The limiting amplitude principle. *Comm. Pure Appl. Math.* 15 (1962), 349–361.
- [37] MORAWETZ, C. S., RALSTON, J. V., AND STRAUSS, W. A. Decay of solutions of the wave equation outside nontrapping obstacles. *Comm. Pure Appl. Math.* 30, 4 (1977), 447–508.
- [38] MORAWETZ, C. S., RALSTON, J. V., AND STRAUSS, W. A. Correction to: “Decay of solutions of the wave equation outside nontrapping obstacles” (CPAM 30 (1977), no. 4, 447–508). *Comm. Pure Appl. Math.* 31, 6 (1978), 795.
- [39] OLSON, D., SHUKLA, S., SIMPSON, G., AND SPIRN, D. Petviashvili’s method for the Dirichlet problem. *J. Sci. Comput.* 66, 1 (2016), 296–320.
- [40] PELINOVSKY, D. E., AND STEPANYANTS, Y. A. Convergence of Petviashvili’s iteration method for numerical approximation of stationary solutions of nonlinear wave equations. *SIAM J. Numer. Anal.* 42, 3 (2004), 1110–1127.
- [41] PETVIASHVILI, V. I. Equation of an extraordinary soliton. *Fizika Plazmy* 2 (May 1976), 469–472.
- [42] PLANCHON, F., AND VEGA, L. Bilinear virial identities and applications. *Ann. Sci. Éc. Norm. Supér. (4)* 42, 2 (2009), 261–290.
- [43] ROUDENKO, S., WANG, Z., AND YANG, K. Dynamics of solutions in the generalized Benjamin-Ono equation: a numerical study. *J. Comp. Phys.* 445 (2021), 110570.
- [44] SANZ-SERNA, J. M., AND CALVO, M. P. *Numerical Hamiltonian problems*, vol. 7 of *Applied Mathematics and Mathematical Computation*. Chapman & Hall, London, 1994.
- [45] SANZ-SERNA, J. M., AND VERWER, J. G. Conservative and nonconservative schemes for the solution of the nonlinear Schrödinger equation. *IMA J. Numer. Anal.* 6, 1 (1986), 25–42.
- [46] WEIDEMAN, J. A. C., AND HERBST, B. M. Split-step methods for the solution of the nonlinear Schrödinger equation. *SIAM J. Numer. Anal.* 23, 3 (1986), 485–507.
- [47] WEINSTEIN, M. I. Nonlinear Schrödinger equations and sharp interpolation estimates. *Comm. Math. Phys.* 87, 4 (1982/83), 567–576.
- [48] WILCOX, C. H. Spherical means and radiation conditions. *Arch. Rational Mech. Anal.* 3 (1959), 133–148.
- [49] YANG, K., ROUDENKO, S., AND ZHAO, Y. Blow-up dynamics and spectral property in the L^2 -critical nonlinear Schrödinger equation in high dimensions. *Nonlinearity* 31, 9 (2018), 4354–4392.
- [50] YANG, K., ROUDENKO, S., AND ZHAO, Y. Blow-up dynamics in the mass super-critical NLS equations. *Phys. D* 396 (2019), 47–69.

LAGA, UMR 7539, INSTITUT GALILÉE, UNIVERSITÉ SORBONNE PARIS NORD
Email address: landoulsi@math.univ-paris13.fr

DEPARTMENT OF MATHEMATICS & STATISTICS, FLORIDA INTERNATIONAL UNIVERSITY, MIAMI, FL 33199, USA
Email address: sroudenko@fiu.edu

DEPARTMENT OF MATHEMATICS & STATISTICS, FLORIDA INTERNATIONAL UNIVERSITY, MIAMI, FL 33199, USA
Email address: yangk@fiu.edu